EVOLUTION OF TEXTURE AND MICROSTRUCTURE DURING THE INITIAL STAGES OF DEFORMATION IN THREE Ni-Co ALLOYS

By

PINAKI PRASAD BHATTACHARJEE

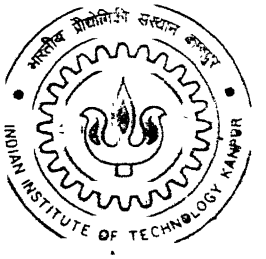

DEPARTMENT OF MATERIALS AND METALLURGICAL ENGINEERING

Indian Institute of Technology Kanpur

FEBRUARY, 2002

EVOLUTION OF TEXTURE AND MICROSTRUCTURE DURING THE INITIAL STAGES OF DEFORMATION IN THREE Ni-Co ALLOYS

A Thesis Submitted
In Partial Fulfillment of the Requirements
For the Degree of

MASTER OF TECHNOLOGY

By
PINAKI PRASAD BHATTACHARJEE

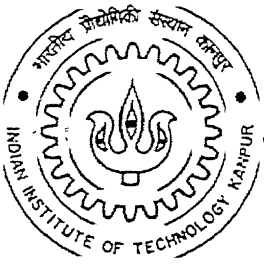

DEPARTMENT OF MATERIALS AND METALLURGICAL ENGINEERING

INDIAN INSTITUTE OF TECHNOLOGY KANPUR

FEBRUARY, 2002

ABSTRACT

An attempt has been made to investigate the phenomenon of texture transition in a series of Ni-Co alloys with widely varying stacking fault energy (SFE). For this purpose three alloys such as Ni-30Co, Ni-40Co and Ni-60Co were cold rolled to 50% thickness, homogenization annealed at 820°C for 3 hours, again cold rolled to 50% reduction and annealed at 820°C for 3 hours to yield the starting materials. These starting materials were further cold rolled to20% and 35% reduction in thickness. Optical and electron microscopy was carried out to investigate the microstructural changes during deformation. Crystallographic texture in the form of ODFs was measured using a fully computer controlled scanning electron microscope (SEM) in the orientation imaging mode.

The deformation textures of the three alloys are totally different one from the other right from the very beginning of deformation. The Ni-30Co alloy shows the development of a strong Cu component, which is characteristic of pure metal type texture, while the Ni-60Co alloy develops a strong Brass (B_s) component, which is characteristic of alloy type texture. The texture of Ni-30Co alloy appears to be of transition type lying in between the two extremes. Fine, closely spaced deformation twins appearing in 'bundles' are observed in Ni-60Co alloy at 20% and 35% deformation as opposed to the Ni-30Co and Ni-40Co alloy at these deformation levels. However, the volume fraction of the twinned region has been found to be rather small compared to the bulk material. These observations tend to negate Wassermann's twin hypothesis for explaining texture transition in f.c.c. metals and alloys.

CONTENTS

ACKNOWLEDGEMENT

At the outset I would like to convey my deepest sense of gratitude to my thesis supervisor Prof. R.K. Ray without whose support, inspiration, prudence and able guidance it could never have been completed. Prof. Ray was more than a thesis supervisor through the course of my M. Tech study. I cherish every moment I have spent with him during this period. He made my stay at IIT Kanpur a home away from home.

I sincerely acknowledge the help and support rendered by Dr. M.N. Mungole to allow me to use some of the facilities of the Metallography Laboratory.

My sincere thanks are also due to Prof. S. Sangal for kindly allowing me to use the ISOMET cutter of his laboratory during the initial preparation of the samples of this study.

I would like to convey my sincere thanks to Mr. V. Kumar for extending all possible and sincere help through the course of this study and I feel very fourtunate to have a laboratory assistant like him in our laboratory.

My sincere thanks are due to Dr. Gauthama and Mr. S.C. Barthwal for their active co-operation during the tedious period of TEM study.

Finally I would like to mention those integral part of my IIT life, my friends, who have made every moment of stay here at IITK to rejoice in future. The list is endless, still, the support, cooperation and help rendered by my laboratory partners Suhash, Arijit, Krishnendu and Deepti and my batch mate Subho, Bikas, John, Debu, Tapas, Sagnik, Amlan, Arnab, Phalguni can never be forgot.

CHAPTER – 1
INTRODUCTION

In f.c.c. metals and alloys usually three different types of deformation texture are found: (i) α-brass or alloy type texture in low stacking fault energy materials; (ii) copper or pure metal type in materials of medium stacking fault energy and (ii) aluminum type texture in very high stacking fault energy materials. While in the brass type only the brass component {110}<112> is present as opposed to the copper type where the Cu {112}<111>, S {123}<634> and brass components are nearly equally strong, the S component predominates in the aluminum type.

It has long been established that the stacking fault energy (SFE) plays a very important role in developing the deformation texture in f.c.c. metals and alloys and this forms a classical topic in texture research. Although a number of theories exists in literature to explain the phenomenon of transition of texture from pure metal type to brass type in low SFE f.c.c. alloys but there seem to be lack of agreement as a whole on this aspect

Excepting Cu, Ag and Au extensive data on SFE is available for two other f.c.c. metals, namely, aluminum and nickel. A reasonable value for the SFE of Ni is ~ 250 ergs/cm^2 and it is appropriate to say that the SFE of nickel is reasonably high. As far as Ni-Co system is concerned it is interesting to note that the SFE of the alloy can be controlled simply by varying the Co content in the alloy. So it is ideally suited for studying the development of deformation texture in f.c.c. alloys with varying SFE. Work on this system is expected to throw much light on the whole phenomena of deformation texture and transition of texture from pure metal type to alloy type.

The subject of texture transition has been studied in great detail in numerous Cu-base alloys. However, similar work on the Ni-Co system, which also shows texture transition, is completely lacking. It was therefore decided to study the different alloys of Ni-Co with varying Co content, such as Ni-30Co, Ni-40Co and Ni-60Co. Previous work on these alloys shows that the Ni-30Co shows a pure metal type texture whereas Ni-60Co shows an alloy type texture. The texture of Ni-40Co is of transition type

In this thesis an attempt has been made to determine what kind of deformation texture forms in these three alloys during the very initial stages of deformation. This is expected to throw light on the existing theories of texture transition in f.c.c. metals and alloys.

CHAPTER – 2
LITERATURE REVIEW

2.1 The Cold Worked State

Generally the cold worked state may be defined as any strained or damaged condition of a crystalline material brought about by processes such as plastic deformation in metal working processes, particle bombardment, quenching from a sufficiently high temperature or phase transformations [2]. The defects that are generally associated with a cold worked material may be grouped in three classes, namely, (1) point defects such as vacancies and interstitials, (2) linear defects mainly the dislocations (3) planar defects like stacking faults and (4) volume defects mainly voids. In the present work cold worked state brought about by plastic deformation will only be considered, with reference to f.c.c metals and alloys. Plastic deformation is accompanied by a change of dimension of the material under stress beyond its elastic limit. Any or all of the defects may be produced in a plastically deformed material. If the deformation is carried out at a low temperature depending upon the material being considered many of these defects will be retained in the material. In cold worked condition the dislocation density of a material is much higher compared to the material in undeformed condition. Plastic deformation produces an increase in the umber of dislocations, which by virtue of their interactions results in a higher state of internal stress

2.1.1 Cold Worked Structure

Considerable detailed knowledge on the cold-worked state has been obtained from thin-film electron microscopy. Baily and Hirsch [2,3] made electron microscopic observations on polycrystalline silver, copper and nickel foils deformed in tension. They found that the dislocations are arranged in a cellular structure. The cell boundaries appear to consist of complex dislocation arrangements together with a large number of small loops. The misorientation across cell walls were measured and found to be of the order of a few degrees. With increasing deformation the dislocation density and misorientation across cell- boundaries in heavily deformed specimens (cold-rolled to 95% reduction) have been found to be quite large, even upto ~10°. Due to very high dislocation density ($>10^{11}$) present at this stage the individual dislocations are not easily resolved, and it is

always very difficult to recognize the original grain boundaries. This is also confirmed by Bollman's study [4] on nickel cold rolled to 80% deformation.

Weissman et.al. [5] have reported observations on the microstructure of high purity aluminum which was cold rolled to different amounts. Their result indicate that for a weakly deformed (5% cold rolled) specimen the microstructure consists of long kinked dislocation lines which upon interaction form dislocation tangles. Increased cold-working to 10% reduction by rolling, gives rise to a more pronounced dislocation entanglement and a distinct emergence of a cell structure. At about 30% of cold-reduction. the formation of cell structure is well advanced, with most of the dislocation tangles arranged in the cell walls and relatively few dislocations within cell walls. The cell walls become more sharply delineated with increasing deformation.

2.1.2 Deformation of FCC Crystals

The stress strain curve of a single crystal has been shown in Figure 2.1 and three regions of hardening have experimentally been verified. Stage I, the region of easy glide is a region, is a stage in which the crystal undergoes little work-hardening. In the easy glide region dislocations can move relatively large distance without encountering barriers. During easy glide slip is found to occur on a single slip system and as a result slip this region has often been termed as *laminar flow*.

In the stage II region or linear hardening region the work-hardening increases in a linear fashion. In this stage slip occurs on more than one slip system and due to complex interaction between dislocations moving on different slip systems and this gives rise to increasing work-hardening. In stage II the ratio of work-hardening coefficient ($d\tau/d\gamma$) to that of shear modulus is of the same order of magnitude ($\approx$ 1/300) for all fcc metals. Dislocations tangles begin to develop that finally results in dislocation cell structure characterized by regions almost free of dislocation surrounded by region of high dislocation density.

Stage III is the region of decreasing rate of strain hardening. The processes occurring in this stage are often called *dynamical recovery*. In this part of the stress-strain

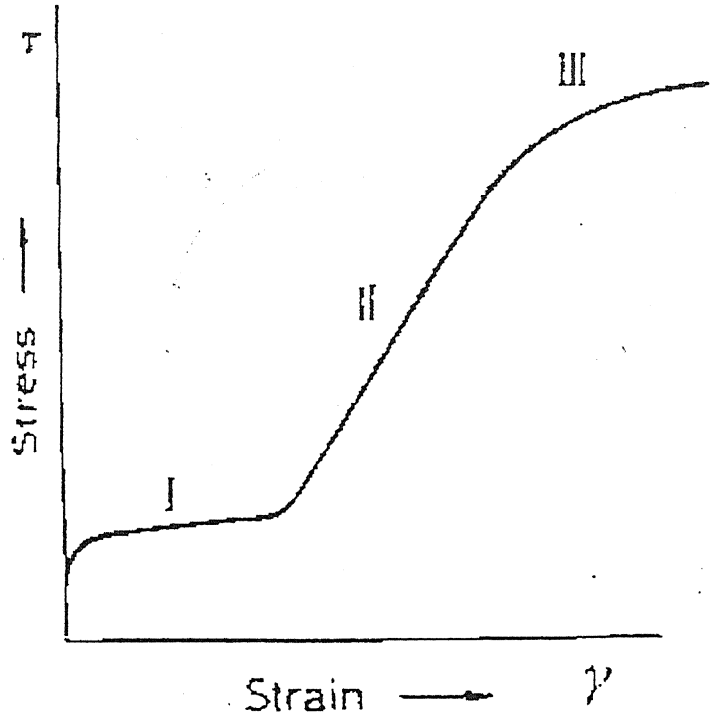

Figure 2. 1. Stress strain curve showing the three stage hardening behavior of f.c.c. single crystals [Ref: R.E. Smallman and R.J. Bishop, 'Metals and Materials', p. 237, (1995), Butterworth-Heinemann, UK)].

curve the stress becomes high enough so that the dislocation can take part in processes that are suppressed at lower stresses. Cross slip is the principal mechanism by which the dislocation piled up at barrier can escape and thereby reduce the internal strain field. The initiation of stage three is temperature dependent.

The low stacking fault energy metals exhibit all three work-hardening stage at room temperature, but metals with a high stacking fault energy often shows only two stages of hardening. It is found for example that at 78 K aluminium behaves like copper at room temperature and exhibits all three stages, but at room temperature and above, stage II is not clearly developed and stage III starts before stage II becomes at all predominant. This difference between aluminum and noble metals is not only due to their difference in their melting point but also to the difference in stacking fault energies which affects the width of extended dislocation. The main effect of a change of temperature of deformation is, however, a change in the onset of stage III; the lower the temperature of deformation, the higher is the stress corresponding to the onset of stage III.

Because the flow stress of a material may be affected by a change of temperature or strain-rate it has been found convenient to think of the stress as made up of two components according to

$$\tau = \tau_s + \tau_g \qquad (2.1.2.1)$$

where τ_s is that part of the flow stress which is dependent upon temperature, and τ_g is a temperature-independent contribution. The relative importance of τ_g and τ_s can be studied conveniently by measuring the dependence of flow stress on temperature or strain rate, i.e. the change in flow stress $\Delta\tau$ on changing the temperature or strain rate, as function of deformation.

The stage I easy glide region in cubic crystals, with its small linear hardening, corresponds closely to the hardening of cph crystals where only one glide plane operates. It occurs in crystals oriented to allow only one glide system to operate. In this case slip distance is large, of the order of specimen diameter, with the probability of dislocations slipping out of the crystal. Electron microscope observations have shown that the slip lines on surface are very long ($\approx$ 1 mm) and closely spaced, and that the slip steps are small corresponding to the passage of only a few dislocations. It is also to be expected

that the flow stress in easy glide will be governed by the ease with which sources begin to operate, since there is no slip on a secondary slip system to interfere with the movement of primary glide dislocations.

As soon as another glide system becomes operative there is a strong interaction between dislocations on the primary and secondary slip systems, which gives rise to a steep increase in work-hardening, and turbulent flow begin, when the crystal reaches an orientation for which two or more slip systems are equally stressed. This situation leads to a high resolved stress on the secondary slip system, and its operation gives rise to those lattice irregularities which cause some dislocations to become stopped inside the crystal. The transformation to stage II then occurs.

The characteristic feature of deformation in stage II is that slip takes place on both the primary and secondary slip systems. As a result, several new lattice irregularities are formed which will include (1) forest dislocations (2) Lomer-Cottrell barriers, and (3) jogs produced either by moving dislocations cutting through the forest dislocations or by forest dislocations cutting through source dislocations. Consequently, the flow stress τ may be identified, in general terms, with a stress which is sufficient to operate a source and then move the dislocations against (1) the internal elastic stress from the forest dislocations, (2) the long range stresses from groups of dislocation piled up at barriers, and (3) frictional resistance due to jogs. In a cold-worked metal all these factors nay exist to some extent, but because a linear hardening behavior can be derived by using any one of the various contributory factors, there have been several theories of stage II hardening, namely (1) the pile up theory, (2) the forest theory and (3) the jog theory. All have been shown to have limitations in explaining various features of the deformation process, and have given way to a more phenomenological theory based on direct observations of the dislocation distribution during straining.

In stage II it is proposed that dislocations are proposed that dislocations are stopped by elastic interaction when they pass too close to an existing tangled region with high dislocation density. The long-range internal stresses due to dislocations piling up behind are partially relieved by secondary slip, which transforms the discrete pile-up into a region of high dislocation density containing secondary dislocation network and dipoles. These region of high dislocation density act as new obstacles to dislocation glide, and since every new obstacle is formed near one produced at a lower strain, two-

dimensional network structures are built up forming the walls of an irregular cell structure. With increasing strain the number of obstacles increases, the distance a dislocation glides decreases and therefore the slip line length decreases in stage II. The structure remains similar throughout stage II but is reduced in scale. The obstacles are in the form of ribbons of high densities of dislocations which, like pile-ups, tend to form sheets. The work-hardening rate depends mainly on the effective radius of the obstacles, and this has been considered in detail by Hirsch and co-workers [6] and shown to be a constant fraction k of the discrete pile-up length on the primary slip system. In general work-hardening rate is given by $\theta_{II} = k\mu/3\pi$ and for an fcc crystal the small variation in k with orientation and alloying element is able to account for the variation of θ_{II} with those parameters.

The dislocation arrangement in metals with other structures is somewhat similar to that of copper with differences arising from stacking fault energy. In Cu-Al alloys the dislocations tend to be confined more to the active slip planes, the confinement increasing with decreasing stacking fault energy. In stage I dislocation multiples are formed as a result of dislocations of opposite sign on parallel nearby slip planes 'paring up' with one another. Most of these dislocations are primaries. In stage II the density of secondary dislocation are much less ($\approx 1/3$) than that of the primary dislocations. The secondary slip occurs in bands. And in each band slip on one particular slip on one particular secondary plane predominates. In niobium, a metal with high stacking fault energy, the dislocation distribution is rather similar to copper. In Mg, typical of cph metals, stage I is extensive and dislocations are mainly in the form of primary edge multipoles, but forest dislocations threading the primary slip plane do not appear to be generated.

The dislocation structure developed during the deformation of fcc and bcc polycrystalline metals follows the same general pattern as that in single crystals; primary dislocations produce dipoles and loops by interaction with secondary dislocations, which give rise to local dislocation tangles gradually developing into three dimensional networks of sub boundaries. In bcc metals, and fcc metals with high stacking fault energy, the tangles rearrange into sharp boundaries but in metals with low stacking fault energy the dislocations are extended, cross slip is restricted, and sharp boundaries are not formed even at large strains. For a given dislocation distribution the flow stress is found to vary with the dislocation density (ρ) according to

$$\tau = \tau_0 + \alpha\mu b\rho^{1/2} \qquad (2.1.2.2)$$

Where μ is the shear modulus; α is a constant at a given temperature ≈ 0.5; τ_0 for fcc metals is zero as shown in Figure 2.2. Grain boundary also affects work-hardening by acting as barriers to slip from one grain to next. In addition, the continuity criterion of polycrystals enforces complex slip in the neighbourhood of the boundaries which spreads across the grains with increasing deformation. This introduces a dependence of work-hardening rate on grain size which extends to several percent elongations. After this stage the work hardening rate becomes independent of grain size and found for many fcc polycrystals is about $\mu/40$.

The dependence between grain size and the stress to initiate plastic flow, σ_y, is found to obey the Hall-Petch relation given by

$$\sigma_y = \sigma_0 + kd^{-1/2} \qquad (2.1.2.3)$$

where d is the average grain size; σ_0 is the frictional stress which is independent of grain size and represents the stress needed to move unlocked dislocations in slip plane of a single crystal.

2.1.3 Cold Working – Theoretical Treatment

The properties of a material are altered by cold-working, i.e. deformation at a low temperature relative to its melting point, but not all the properties are improved, for although the tensile strength, yield strength and hardness are increased, the ductility and general ability to deform decreases as in Figure 2.3. Moreover, the physical properties such as electrical conductivity, density and others are lowered. Of these many changes in properties, perhaps the most outstanding are those that occur in mechanical properties; the yield stress of the mild steel for example, may be raised by cold work from 170 up to 1050 MN/m^2.

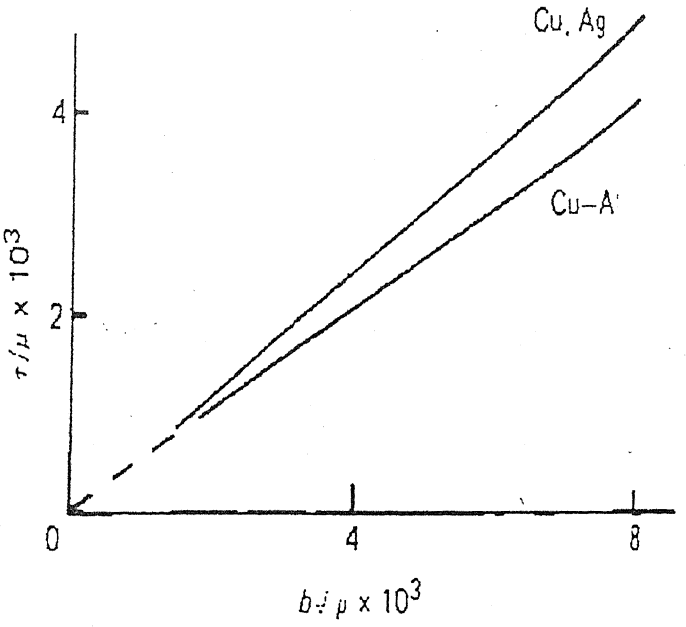

Figure 2.2. Dependence of flow stress on (dislocation density)$^{1/2}$ for Cu, Ag and Cu-Al [Ref: R.E. Smallman and R.J. Bishop, 'Metals and Materials', p. 236, (1995), Butterworth-Heinemann, UK)].

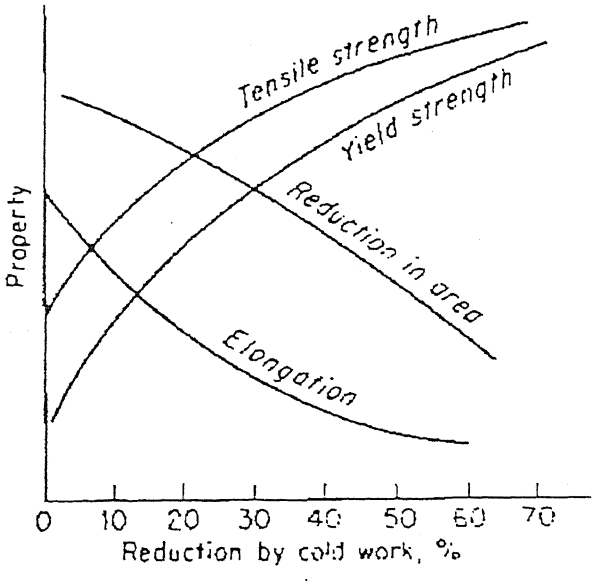

Figure 2.3. Variation of tensile properties with amount of cold work [Ref: G.E. Dieter, 'Mechanical Metallurgy', p. 232, (1988), McGrawhill Book Co., UK].

Such changes in mechanical properties are, of course, of interest theoretically, but they are also of great importance in actual industrial practice. This is because the rate at which the material hardens during deformation influences both the power required and the method of working in various shaping operations, while the magnitude of the hardness introduced governs the frequency with which the component must be annealed to enable further working to take place.

Many theories of work hardening, based upon direct electron-microscopic observation of dislocations, have been proposed in recent years, but none of them has been recognized as the generally accepted one. The reason should be sought in the fact that the processes associated with plastic deformation are highly complicated and diverse. All these theories are however important and essential, since they, can firstly provide the basis for more purposeful experimenting; secondly can provide basic information about the stress-strain curve and answer the exact mechanism of plastic deformation and factors which control them.

During plastic deformation, dislocation movement is impeded by a number of factors, the principal among them are as follows:

(1) stress field produced by other dislocations;

(2) boundaries of grains and sub-grains, solute atoms, particles of other phases, and surface films.

Since plastic flow occurs by a dislocation mechanism the fact that work-hardening occurs means that it becomes difficult for dislocation to move as the strain increases. All theories of work-hardening depends on this assumption, and the basic idea of hardening put forward by Taylor in 1934, is that some dislocation become stuck inside the crystal and act as source of internal stress which opposes the motion of other gliding dislocations. Other principal assumptions in the theory are that many dislocations do not reach the surface of a crystal, but interact elastically with other dislocation within the crystal and become anchored, forming a network; deformation is affected by movement of individual dislocations.

A simple way in which two dislocations could become stuck is by elastic interaction. Thus, two parallel dislocation of opposite sign moving on parallel slip planes in any sub grain may become stuck as a result of elastic interaction. Taylor assumed that dislocation become stuck after traveling an average distance, L, while the density of

dislocation reaches ρ, i.e. work-hardening is due to the dislocations getting in each other's way. The flow stress is then the stress necessary to move a dislocation in the stress field of those dislocations surrounding it. This stress τ is generally given by

$$\tau = \alpha\mu b/l \qquad .(2.1.2.4)$$

Where μ is the shear modulus, b the berger's vector, l the mean distance between dislocations which is $\approx \rho^{-1/2}$, and α a constant; in the Taylor's model $\alpha = 1/8\pi(1-\nu)$. Figure 2.2. shows such a relationship for Cu-Al single crystal and polycrystalline Ag and Cu.

In his theory Taylor considered only a two-dimensional model of a cold worked metal. However, because plastic deformation arises out from the movement of dislocation loops from a source, it is more appropriate to assume that when the plastic strain is γ, N dislocation loops of side L (considering that square loops are emitted) have been given off per unit volume. The resultant plastic strain is then given by

$$\gamma = NL^2b \qquad (2.1.2.5)$$

and l by

$$l = [1/\rho^{1/2}] = [1/4LN]^{1/2} \qquad (2.1.2.6)$$

Combining these equations, the stress-strain relationship

$$\tau = \text{const.}\ (b/L)^{1/2}\gamma^{1/2} \qquad (2.1.2.7)$$

is obtained. Taylor assumed L to be a constant, i.e. the slip lines are of constant length, which result in a parabolic relationship between τ and γ.

Taylor's assumption that during cold work the density of dislocations increases has been amply verified, and indeed the parabolic relationship between stress and strain is obeyed, to a first approximation, in many polycrystalline aggregates where deformation in all grains takes place by multiple slip. Experimental work on single crystals, shows however, that the work- or strain hardening behavior, and depends not only on crystal structure but also on other variables such as crystal orientation, purity and surface conditions.

The theory of interaction of dislocation complexes (Mott's theory) was developed to modify Taylor's theory for more conformity with experimental evidence. The Mott theory considers the interaction of dislocation groups emanating from a source, rather than of individual dislocations. Dislocations moving in a slip plane become piled up

against obstacles (sessile dislocations), resulting in an increase of the internal stress at the head of the pile-up. A dislocation pile-up consisting of n dislocations is considered as a superdislocation of Berger's vector nb. The separation distance is $2L$ (each section of dislocation line moves a distance L), the distance between slip plane δ, the density of pile-up group is $\rho = 1/(L\delta)$, and the average distance between them is

$$l = 1/\sqrt{\rho} = (L\delta)^{1/2} \qquad (2.1.2.8)$$

Substituting the value of δ for a superdislocation of strength nb, we have:

$$\tau = Gnb/2\pi\,(L\delta)^{1/2} \qquad (2.1.2.9)$$

The plastic strain γ is found by summing up the strain from each pile-up, i.e.

$$\gamma = nbL/\,L\delta = nb/\delta \qquad (2.1.2.10)$$

substituting the value of δ from earlier relation we get a parabolic relationship between τ and γ:

$$\tau = (G/2\pi)\,(\gamma nb/L)^{1/2}. \qquad (2.1.2.11)$$

As has been found later, in most crystals the relationship between τ and γ at stage I and II are linear, rather than parabolic. This is the principal drawback of earlier theories of cold working.

The theory of hardening due to short-range stress field was put forward by J. J. Gilman. According to this proposition a moving dislocation leaves behind dislocation dipoles, each of which is essentially a pair of parallel dislocation of opposite signs. The existence of dislocation dipoles has been confirmed by electron-microscopic examination. Dislocation dipoles interact with subsequent dislocations and inhibit their movement. At heavier deformation, more dipoles are left and more strongly they inhibit dislocation movement.

The crystal structure is important in that single crystal of some hexagonal (cph) metals slip occurs on only one family of slip planes, those parallel to the basal plane, and these metal show a low rate of work-hardening. Cubic crystals on the other hand are capable of undergoing deformation on more than one slip system, and these metal show a strong work-hardening behavior. The influence of temperature depends on the stress level reached during deformation and also on other factors which must be considered in greater detail. However, even in cubic crystals the rate of work-hardening may be extremely small if the crystal is restricted to slip on a single slip system. Such behavior strongly

suggests that strong work-hardening is caused by the mutual interference of dislocations gliding on intersecting slip systems. The work-hardening behavior in metals with a cubic crystal structure is more complex than in most other structures because of the presence of a greater number of possible slip systems, and it is for that reason that much of the experimental evidence is related to these metals, particularly those with a fcc structure.

2.1.4 The Stored Energy Produced During Cold Working

A small percentage (usually from 1% to 10%) of the energy expended in plastically deforming a metal remains 'stored' in the metal causing an increase in internal energy. In particular it increases the strain resistance and electrical resistivity, accelerates diffusion process, etc. The stored strain energy is determined as the difference between the work performed in the deformation and the amount of heat evolved, or by measuring the heat liberated during annealing of the deformed metal. The later method makes it possible to determine simultaneously the distribution of crystal lattice distortions in their thermal stability.

This increment in internal energy is associated with the defects generated during deformation and provides the energetic driving force for relaxation processes which occur when the cold-worked metal is subsequently annealed at a higher temperature. The magnitude of the stored energy produced by cold-working is affected by variables such as purity, method of deformation, temperature, grain size and material.

Comparison of calorimetric and metallographic results have shown that the energy of plastic deformation can be stored by the following mechanisms: -

(1) Elastic strain energy

(2) Energy of dislocations

(3) Energy of point defects

(4) Energy associated with stacking faults and twins

(5) Energy associated with the destruction of ordered regions.

The elastic strain energy for filed 75%Au – 25% Ag alloy has been estimated about 3% of the total stored energy by Averbach [7] et.al. Michell and Haig [8,9] have shown that the elastic strain energy for ground nickel is about 12% of stored energy. These findings show very convincingly that the major portion of the stored energy of cold work, at least for pure metals, is due to lattice defects.

In order to arrive at an estimate of the fraction of the stored energy due to dislocations, information is needed on their density and distribution. Annealed metals normally have dislocation densities between 10^6 to 10^8 lines/cm^2, and severely cold-worked metals usually have between 10^{10} to 10^{12} lines/cm^2. The precise distribution of dislocations depends strongly on the metal, its purity and history of deformation.

Both vacancies and interstitial atoms may be considered responsible for at least some energy storage during deformation. Although an estimate of the stored energy due to vacancies can be made from measured resistivity changes, it is difficult to establish in case of interstitial atoms. In many systems these point defects anneal out during or immediately after deformation.

Stacking faults which are formed during plastic deformation can account for an appreciable portion of stored energy, γ, and on temperature of the deformation.

Deformation twins on a fine scale comparable to stacking faults may also contribute significantly to the stored energy.

If originally there exists in a material, either short or long range order to some degrees, then, during plastic deformation, the passage of dislocations through ordered regions will disturb the degrees of order leading to an increase of the internal energy of the system. Similarly, if, during cold-working precipitates and clusters of solute atoms are sheared due to the passage of dislocation through them, the internal energy will again be increased.

The amount of stored energy increases with deformation first quickly then slowly as in Figure 2.4a and the relative absorbed energy (related to the work performed) decreases with increasing deformation as in Figure 2.4b, which indicates that energy is absorbed more intensively in slight deformations (10 percent in Figure 2.4b) while heat

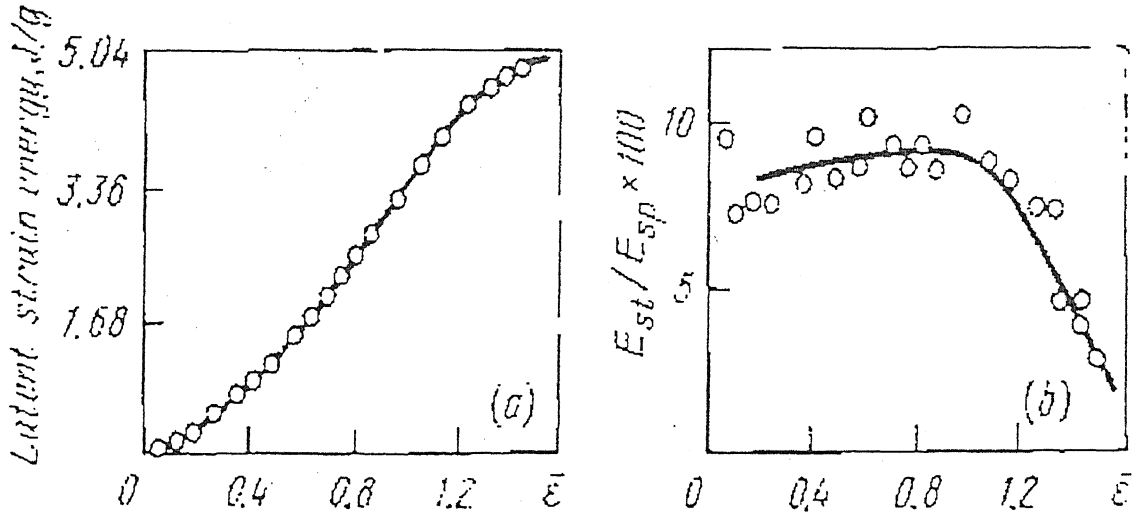

Figure 2. 4. Effect of deformation in torsion on (a) stored (latent) strain energy and (b) the ratio of stored energy E_{st} to spent energy E_{sp} [Ref: P. Polukhin, S. Gorelik and V. Vrontosov, 'Physical Principles of Plastic Deformation', p. 210, (1983), Mir Publishers, Moscow, USSR].

evolution is more substantial on heavier deformations when only 3 percent fall on the energy absorbed. The decrease of the relative absorbed energy with increasing deformation can be explained by the formation of defects in the crystal lattice at the early stages of deformation, which are stable at a given temperature. These defects annihilate partially as the deformation proceeds and liberate free energy in the form of heat. In further deformation, the density of defects increases, and therefore defects of opposite signs are more likely to meet one another and annihilate and even greater portion of the distortions will disappear in the course of deformation. It is expected that a state of saturation will be attained, i.e. the number of distortions formed will be equal to the number of distortions that disappear and the entire energy of deformation will be converted to heat. The fraction of stored energy relative to that spent is 20-25 percent in dynamic plastic working and only 10-15 percent in static as in Figure 2.5. This is an extra indication that lattice distortions appearing in the course of plastic deformation are partially annihilated during this process due to recovery. The effect of elimination of crystal lattice distortions by recovery is substantially lower at low temperatures and slight deformations. Under such conditions, almost the entire energy spent in deformation is absorbed by the metal and spent for the formation of crystal lattice distortions as in Figure 2.6.

2.2 Development of Preferred Orientation or Texture

2.2.1 Introduction

An anistropic arrangement of components of a solid which are orderly oriented relative to an external coordinate system is referred to as *texture*.

In practice, metals and alloys are often found to consist of grains having a stretched fibrous shape. Some alloys may have a lineage arrangement of particles of one or more of their phases. Textures of this type are often called '*mechanical*'. The term implies that the shape of particles of a body and/or their arrangement is anistropic.

Much more common and practically important are *crystallographic textures.* In such a texture, some crystallographic orientations are preferred or, in other words, crystal lattices of some components of a solid have a definite regular orientation in space.

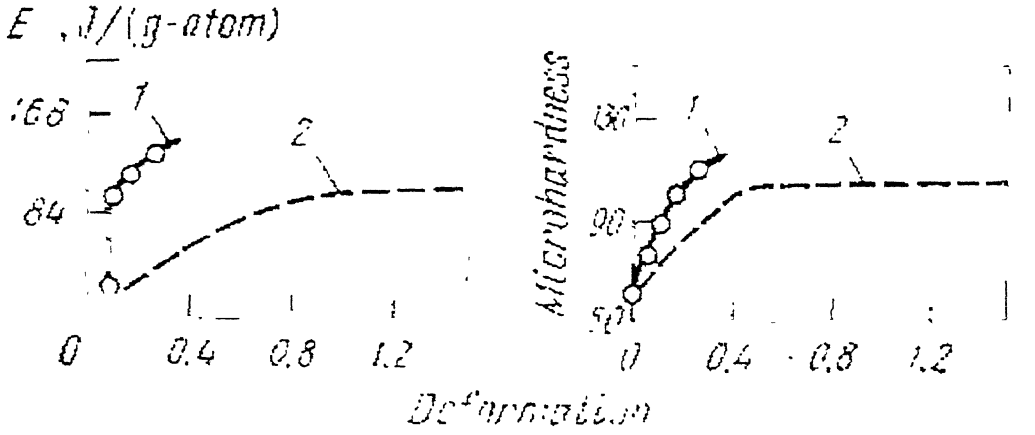

Figure 2. 5. Effect of amount of deformation in (1) high-speed and (2) static plastic working on the stored energy and microhardness of Au-Ag alloy [Ref: P. Polukhin, S. Gorelik and V. Vrontosov, 'Physical Principles of Plastic Deformation', p. 210, (1983), Mir Publishers, Moscow, USSR].

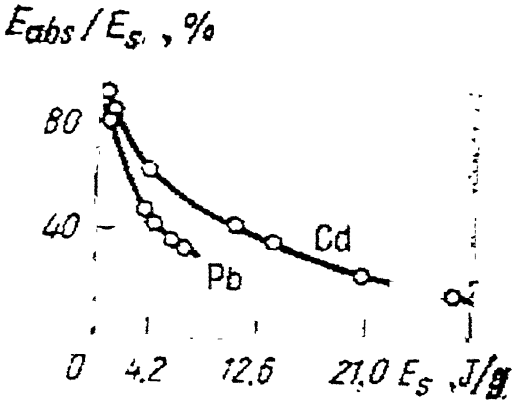

Figure 2.6. Variation of the ratio of absorbed to spent energy in low temperature (77 K) plastic working of cadmium and lead [Ref: P. Polukhin, S. Gorelik and V. Vrontosov, 'Physical Principles of Plastic Deformation', p. 211, (1983), Mir Publishers, Moscow, USSR].

Crystallographic textures are most often found in polycrystalline solids, where some crystals (grains) or their microvolumes may have a preferable crystallographic orientation. When a polycrystalline material is plastically deformed the individual grains tend to rotate into a common orientation. This preferred orientation is developed gradually with increasing deformation, and although it becomes extensive above about 90% reduction in area, it is still inferior to that of a single crystal. The nature of this preferred orientation or the 'texture', which the material acquires, is characteristic of the material itself and also depends on the variable connected with the deformation process. When the material is recrystallized from its cold-worked state the grain rotation again takes place giving rise to a new preferred orientation.

2.2.2 Description of Texture

The most complete description of textures in a polycrystalline material can be given by stating the crystallographic orientation of each and every crystallite belonging to it. But this becomes enormously difficult for a fine-grained polycrystalline metals and alloys where the number of crystallites is very high and therefore, it is customary to use a statistical description instead. X-ray diffraction methods are now widely used to yield a collective determination of orientation over a large number of crystals through scanning and integrating mechanisms. The material is first subjected to X-ray diffraction, and the intensity vs. angle data is recorded. The diffracted intensity data obtained from X-ray techniques are corrected for background intensity and adsorption and then normalized relative to intensity level of a random specimen. Then these dataset are transformed from a linear scale to a polar plot, which is nothing but the pole figure. The dataset may then be represented by the use of either conventional or inverse pole figure or by means of mathematical functions.

Pole figures are simple stereographic projections which show the distribution of particular crystallographic directions in the assembly of grains that constitute the metal. The pole figures must also contain some reference directions and these are usually chosen so that they correspond to easily defined directions in the specimen. In rolled sheet, for example, it is natural to think in terms of the rolling direction (TD) and the sheet plane normal (ND). Figure 2.7(a) shows how the sheet is considered to be situated at the center

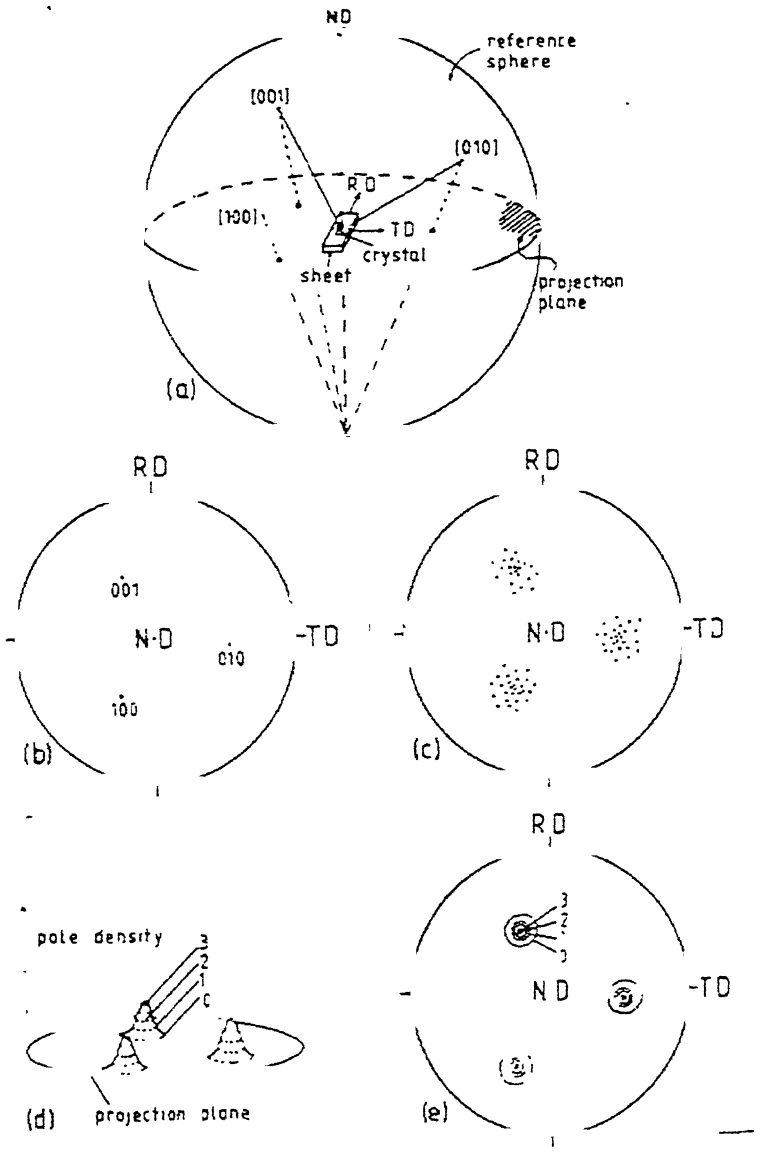

Figure 2.7 (a) Position of the sheet at the center of the stereographic sphere, (b) (100) Pole figure, (c) clustering of pole figure in certain areas revealing presence of preferred orientation or texture, (d) and (e) pole density as contour lines on the stereographic projection [Ref: M. Hatherly and W.B. Hutchinson, 'An Introduction to Textures in Metals, p. 6, (1973), University of Birmingham, UK].

Dedicated to.....

My Parents

Mr. Bijay Krishna Bhattacharjee

&

Mrs. Bandana Bhattacharjee

&

My Lovely Nephew

Abhishek

of a stereographic sphere with the orthogonal reference direction as x, y and z-axes. The orientation of a single grain in the sample can represented by plotting its three {100} poles at the appropriate angular positions relative to the reference directions. In reality all the poles concerned are projected on to the equatorial plane to produce a stereographic projection as shown in Figure 2.7(b). The result is a pole figure and in this specific case it is referred to as a (100) pole figure, showing the positions of the {100} poles for the grain and. therefore, the orientation of grain in the sheet. For a polycrystalline sample all the grains must be considered and three {100} poles must be plotted for each to give the pole figure. If the resulting poles are distributed uniformly over the area of the projection there is no preferred orientation and the specimen is said to have a *random* texture. In real metals this condition is most unlikely to occur and the poles tend to cluster together in certain areas of pole figure to produce texture as shown in Figure 2.7(c). The number of grains is such that the determination of individual orientations is impractical and the plotting of individual grains impossible as has been stated earlier.

To overcome these difficulties it is usual to collect data from many grains simultaneously and to present this in the form of density distribution contours on the pole figure. Figure 2.7(d) and (e) shows how the pole density data may be visualized and presented as contour lines on the stereographic projection. The density values are expressed relative to that which could be expected for a specimen having a random orientation. Contour levels greater than 1 x random imply a concentration of poles and those with less than 1 x depletion in the direction concerned. If a correct average is taken over the whole pole figure the mean density of poles must be 1 since the total number of poles is an aggregate unchanged by the existence of the degree of texture.

The stereographic projection in Figure 2.8(a) shows the three poles of a single grain in a steel sheet. One of the poles is parallel to RD (Rolling Direction) and each of the others lies in the plane perpendicular to RD and at 45° to both ND (Normal Direction) and TD In this single grain a <110> direction is parallel to ND and another <110> direction parallel to TD The orientation of the grain is defined by the pole figure but it can also be described if the crystallographic directions parallel to any two of the three reference directions are specified. By convention the direction chosen are ND and RD

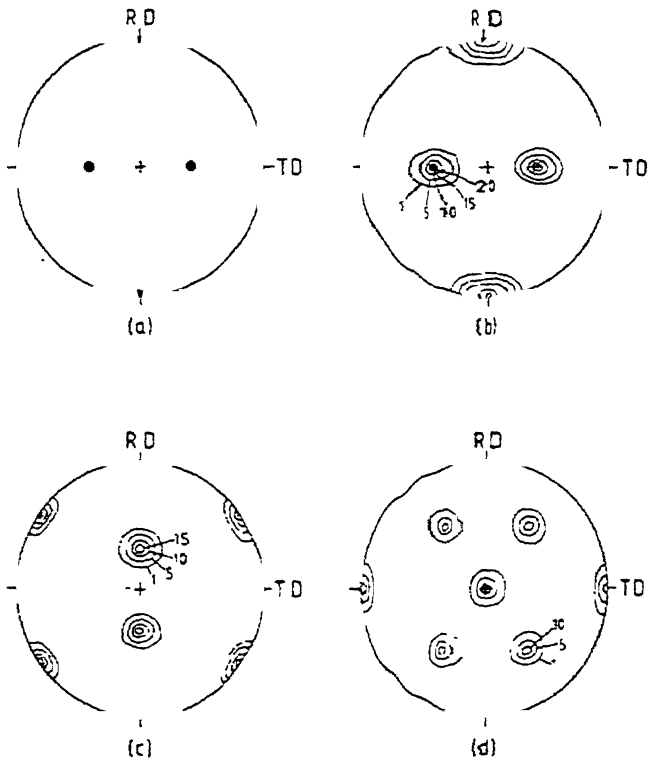

Figure 2.8 (a) <100> poles for the orientation {1 1 0} <001> (b) (100) pole figure for Goss oriented silicon-iron, (c) (1 1 1) pole figure for same material as (b), (d) (1 1 0) pole figure for same material as (b) [Ref: M. Hatherly and W.B. Hutchinson, 'An Introduction to Textures in Metals, p. 6, (1973), University Of Birmingham, UK].

and the description are made in the form {hkl}<uvw>. This states that a plane of the form {hkl} is parallel to the rolling plane (i.e. it's pole is parallel to ND) and that a direction of the form <uvw> is parallel to RD. The orientation of the grain shown in the pole Figure of 9(a) is of the form {110}<001>. It will be apparent that the direction <uvw> must always lie in the plane {hkl}. Real textures are never perfect and Figure 2.8(b) shows the distribution of {100} poles in a grain oriented silicon sheet of the type used in electrical work. The poles are obviously clustered together in positions near the orientation {110}<001> and in this case the notation provides an adequate alternative to the pole figure as a description of the texture present in the steel.

The pole figures given in foregoing figures have all shown the distribution of {100} poles but there is no need for restriction of this type. The {110}<001> orientation of the single grain shown in Figure 2.8(a) can be described just as well by defining the positions of the {110} plane normals or the {111} normals or indeed the normals of any crystallographic plane. Figure 2.8(c) and 9(d) show the corresponding (111) and (110) pole figures for the steel sheet used to obtain Figure 2.8(b). The pole figures are markedly different but each describes the texture of the same steel sheet. But the simplest pole figures will be those depicting the distribution of poles of planes with the lowest multiplicity and the usual pole figures refer to {100}, {110}, {111} and sometimes {2111} planes. Reflections are not obtained from (100) planes for either bcc or fcc cubic metals and so the second order (200) reflections must be measured. Since it is usual to refer to the pole figure in terms of the measured reflection, bcc textures are described by (110), (200), (112), (222), etc., pole figures while fcc textures are interpreted on the basis of (111), (200) and (220) pole figures. Obviously there is no difference between pole figures from first and second order reflections as the poles are identical for the two cases.

While the pole figures provides a description of texture it must be interpreted. Even in the simple case of Figure 2.8 the description of the texture by the indices {110}<001> is incomplete and over simplified. It is possible to exhibit all the texture component of a material by pole figure but the main limitation is that it is scattered through out a zone, and quite naturally different texture components overlap, and it becomes difficult to distinguish them effectively. Also the resolution of the pole figure is somewhat poor and gives a qualitative idea about the strength of a particular texture component.

A complete description of texture of the texture would be provided by a function that described the orientation of all the crystallite in the metal. Such *orientation distribution functions* (ODFs) can now be determined and are extremely valuable for purposes of quantative analysis. ODFs describe the frequency of occurrence of particular orientations in a three-dimensional (Euler) orientation space. This space is defined by three Euler angles, which constitute a set of three consecutive rotations that bring the crystallographic <100> axes of each crystallite into coincidence with the specimen axes. If one denotes by dV the total volume of all the elements which possess the orientation g within the infinitesimal orientation range dg, and by V the whole sample volume, then the ODF, f(g), is defined by $dV/V = f(g)dg$, where $dg = (1/8\pi^2)\ \mathrm{Sin}\varphi\ d\varphi_1\ d\varphi\ d\varphi_2$. Here, φ_1, φ and φ_2 are three Euler angles. Mathematical methods have been developed that allow an ODF to be calculated from the numerical data obtained from several pole figures.

The most widely adopted notations employed for the description of ODFs are those proposed independently by Bunge and Roe [10]. They used generalized spherical harmonic functions to represent crystallite distributions while Williams [11] uses an iterative least square solution. The former methods have most widely been adopted. Unfortunately, all the methods employ different definitions and different symbols for the three angles which are used to describe the orientation of a given crystallite. While the Euler angle proposed by Bunge to describe the crystal rotations are, φ_1, φ, φ_2 and the set of angles employed by Roe is referred to as ψ, θ and φ respectively and those proposed by Williams are given by α, ρ and β. The relationship between three sets of angles is given in Table 2.1.

φ_1, φ and φ_2, these three angles in Bunge notation have special significance. It is easily understood that a frame of three mutually perpendicular axes can be superimposed on another frame of three mutually perpendicular axes. The same principal is followed here. The specimen frame as shown in Figure 2.9(a) is superimposed on the crystallographic frames by means of three successive rotations (Figure 2.9(b)). The procedure is as follows:

Table 2.1 Relationship Between Roe, Williams and Bunge Notation [Ref: M. Hatherly and W.B. Hutchinson, 'An Introduction to Textures in Metals, p. 6, (1973), University of Birmingham, UK].

Roe	Bunge	Williams
φ	$\varphi_2 + \pi/2$	α
θ	φ	ρ
ψ	ϕ_1	$\beta = \psi + \tan^{-1}(\tan\alpha + \cos\beta)$

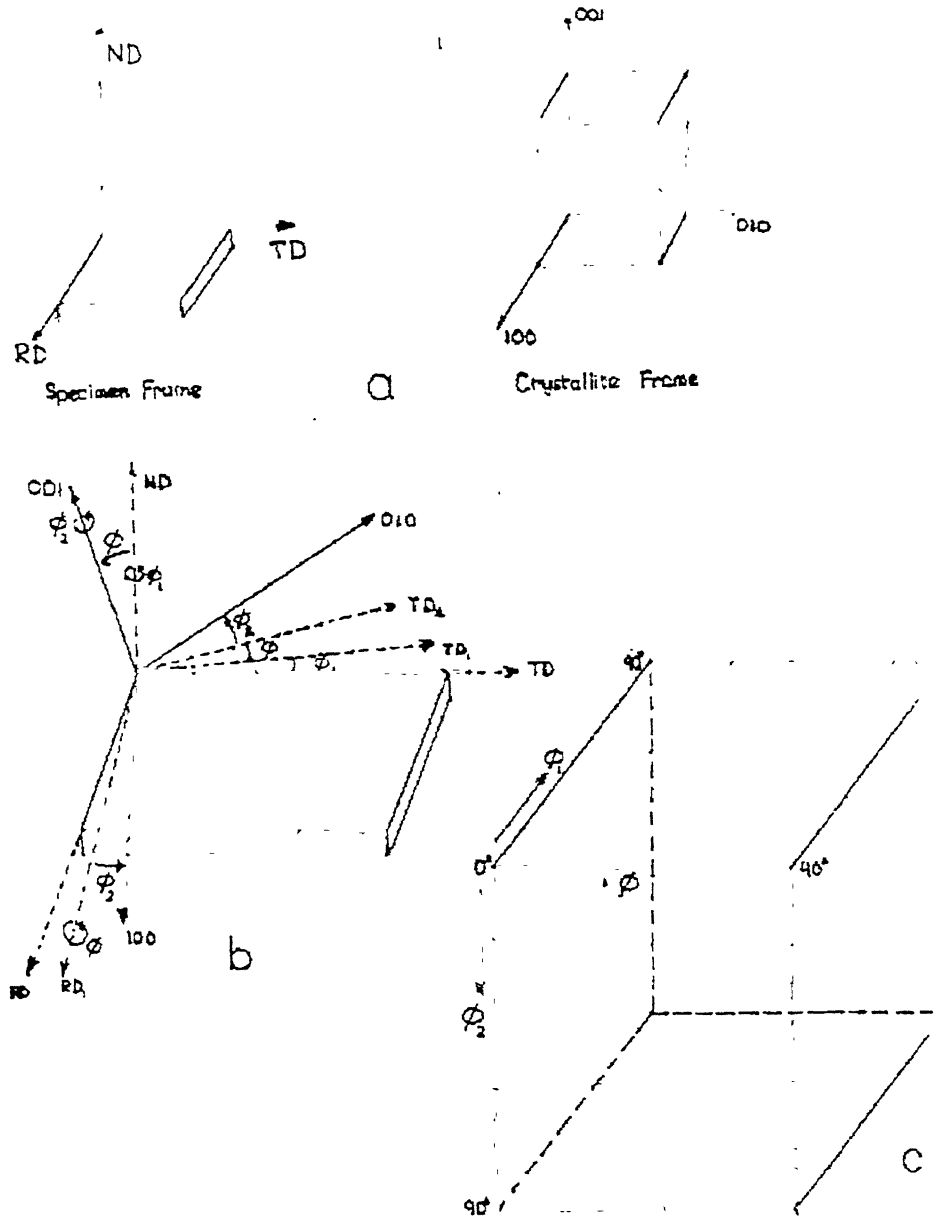

Figure 2.9 (a) Specimen frame and Crystallite frame (b) The three rotations for superimposing crystallite frame on reference frame (c) Orientation space [Ref: M. Hatherly and W.B. Hutchinson, 'An Introduction to Textures in Metals, p. 6, (1973), University of Birmingham, UK].

(1) A first rotation φ_1 around ND transforms TD and RD into the new direction TD_1 and RD_1 respectively. φ_1 has to have such a value that RD_1 will be perpendicular to the plane formed by ND and [001].

(2) A second rotation φ around the new direction RD_1 with φ having such a value that ND is transformed into [001] and TD_1 into TD_2.

(3) The third rotation φ_2 with φ_2 having such a value that RD_1 is transformed into [100] and TD_2 into [010].

So $\varphi_1, \varphi, \varphi_2$; the set of these three angles completely represent the orientation of a particular texture. Immediately for every set of {hkl}<uvw> value there is exactly one set of $\varphi_1, \varphi, \varphi_2$ values. Now depending on this concept, a three-dimensional view of Euler space in the Bunge notation is presented in Figure 2.9(c) where three mutually perpendicular axes represent the values of ϕ_1, ϕ, ϕ_2; from 0° to 90°. A three dimensional view of Euler space in the Bunge notation is presented in Figure 2.10. In this diagram, a few ideal orientations are illustrated, together with the locations of the technologically important RD, TD and ND fibers. The orientations lying along the RD fibers are related rotations around the RD || <110> axis, and the fiber lies along $\varphi_2 = 45^\circ$ in the $\varphi_1 = 0^\circ$ section. The TD fiber contains orientations that have a common <110> || TD and this lies along $\phi_2 = 45^\circ$ in the $\varphi_1 = 0^\circ$ section. Orientations on the ND fiber have a common <111> || ND and this fiber extends parallel to ϕ_1 axis at $\phi = 55^\circ$ and $\varphi_2 = 45^\circ$. The RD and ND fibers have often been called the α and γ respectively.

Two-dimensional views of $\phi = 45^\circ$ and $\varphi_2 = 45^\circ$ sections in the Roe and Bunge notations, respectively, are illustrated in Figure 2.11(a) and (b), in which several ideal orientations are again identified. The quantitative evaluation of texture has been made much easier by the common availability of microcomputers, which had led, in turn, to the rapid and straightforward calculations of ODFs. The much higher resolving power associated with this form of texture representation has enabled researchers to recognize more clearly many details of individual textures, which may appear ambiguous or difficult to identify in a pole figure.

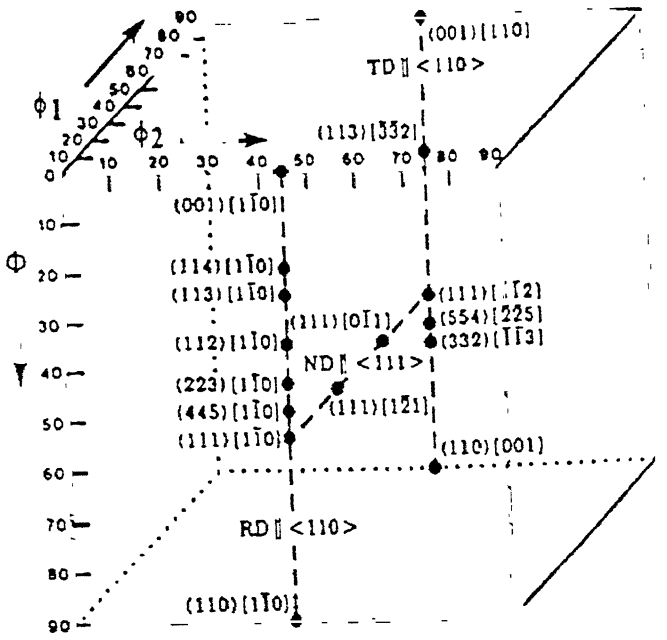

Figure 2.10. A three-dimensional view of Euler space (Bunge notation) [R.K Ray, 'Textures in Metals Research', (Ed.) R.K. Ray and A.K. Singh, p. 309, (1999), Oxford and IBH Publishung Co. Pvt. Ltd., New Delhi, India]

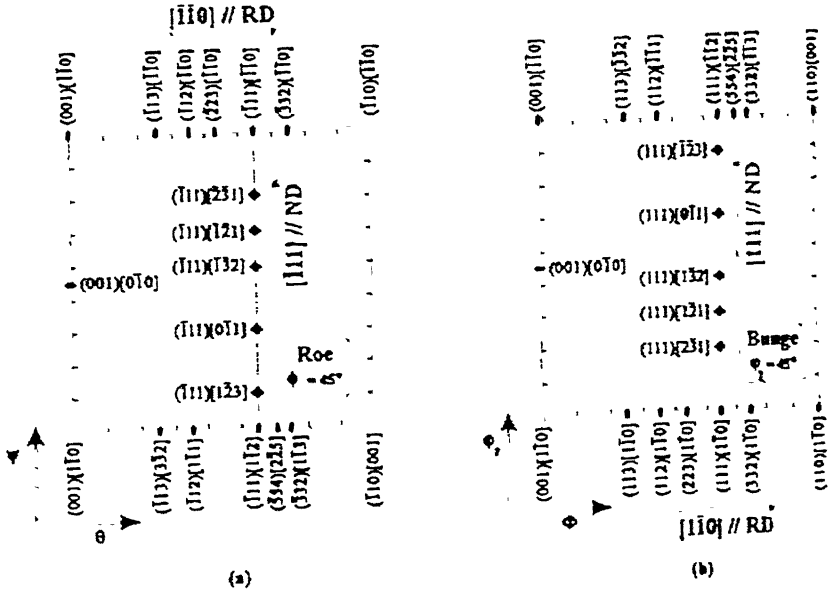

Figure 2.11. Two-dimensional views of (a) $\varphi = 45^0$ section (Roe notation) (b) $\varphi_2 = 45^0$ section (Bunge notation) [Ref R.K. Ray, 'Textures in Metals Research', (Ed) R.K Ray and A.K. Singh, p 310, (1999), Oxford and IBH Publishing Co Pvt Ltd., New Delhi, India]

2.2.3 Experimental Determination of Texture

The vast majority of texture determinations are done using the well-established principle of X-ray diffraction from poly crystals although some alternative techniques are occasionally used. Neutron diffraction offers distinct advantages in certain cases. Methods based on determination of an orientation sensitive physical property such as magnetic torque or elastic modulus may also give some information concerning the texture of a metal. However, such methods are limited scope and better suited for semi-quantitative comparisons of similar materials than to an understanding of the fundamental texture.

2.2.3.1 X-ray Diffraction Method

All the variants of diffraction method use a monochromatic beam of radiation with the Bragg condition fixed for a single set of reflecting planes and maintained throughout the determination of pole figure. Under these condition the normal ($\hat{k}$) to the diffracting planes {hkl} remains fixed in space and the specimen is rotated through a wide range of angles so that many different directions in the sample are brought into coincidence with the diffracting normal. Whenever a crystal becomes so oriented to any one set of the prescribed {hkl} planes coincides with the fixed normal, $\hat{k}$, a diffracted intensity will be measured from that grain. The total diffracted intensity is then proportional to the volume of the specimen in which the {hkl} planes are so oriented. In other words, the measured intensity at a given time, corrected for background and geometrical factor, is directly proportional to the pole density on the pole figure at the position under investigation. The proportionality between diffracted intensity and pole density is usually quantified in 'terms' of the 'random intensity', or the intensity which is observed when a textureless sample is examined under precisely the same conditions. The pole figure is then plotted out with contour levels which correspond to ½, 1, 2, 3.....x random intensity. This provides a sensible basis on which the sharpness of the texture may be assessed and allows a comparison to be made between results obtained in different laboratories and using different experimental methods.

2.2.3.2 The Schulz Reflection Method

In the method devised by Schulz [12] the specimen used is typically a piece of sheet about 25 mm square with a flat surface that has been prepared by chemical polishing or etching. The X-ray beam must not be transmitted through the specimen and so the thickness should normally be greater than ~0.2 mm. When mounted on the Goniometer the specimen is subjected to three type of movement. These are

(i) simple to and fro translation and helps in improving the measurement by increasing the number of grains that are sampled.

(ii) Rotation about an axis perpendicular to the sheet surface (angle ψ), and

(iii) Rotation about an orthogonal axis through an angle φ.

Figure 2.12(a) shows a schematic diagram explaining the geometrical arrangement and the corresponding stereographic projection has been given in Figure 2.12(b).

The main problem associated with this method is that the diffracted intensity is affected by the geometrical setting of the goniometer as well as by the variation in texture that is measured. Also the *defocusing* effect causes a reduction in intensity which is associated with a higher value of the angle φ.

When determining a pole figure from a unknown textured material, it is usual to carry out a run on a 'random' specimen. Since this specimen is essentially textureless any variation in the measured diffraction intensity may be attributed solely due to the defocusing effect and it acts as a corrective measure. More importantly, it provides a logical reference intensity level with which to compare the textured material. Region in the specimen which shows less than the random specimen intensity (< 1 x random) may be considered depleted in poles. The augmented intensity regions are readily quantified by contours of 2 x random, 3 x random...etc. Figure 2.13(a) shows a chart recording of a (111) pole figure from a 95%cold rolled aluminum and demonstrates hoe the random sample is used in plotting procedure. Superimposed on the texture plot is the intensity which was measured from the random sample (labeled 1 x random) which shows the loss of intensity due to defocusing at the higher φ values. A series of reference lines are then drawn which represents multiples and sub multiples of the diffracted intensity from the random sample. To determine these values the diffracted intensity (i.e. total measured

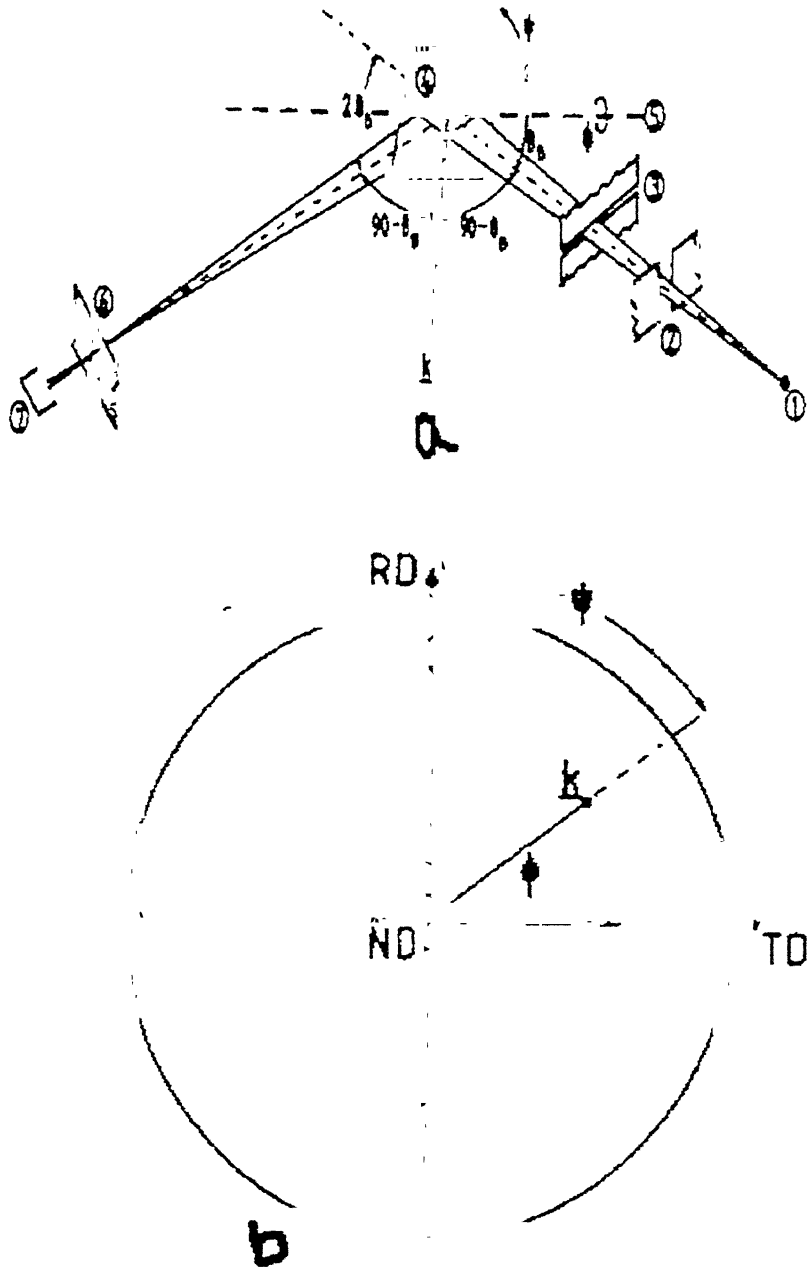

Figure 2.12. (a) Geometrical arrangement of the specimen in the texture Goniometer (b) Corresponding stereographic projection of (a) [Ref: M. Hatherly and W.B. Hutchinson, 'An Introduction to Textures in Metals, p. 22, (1973), University of Birmingham, UK].

intensity minus the background values) is multiplied by n for the n x random level and then background level is added on. When plotting a contour on the pole figure; Figure 2.13(b), marks are made on the spiral path at each point corresponding to the values of φ and ψ where the measured intensity trace cuts the particular reference line concerned. These marks are then joined to give a contour line which separates the areas of the pole figure which are above that reference level from those which are below it. The small letters on the 3 x random level in Figures 2.13(a) and (b) indicate how this information is transferred from the chart to pole figures to produce the 3 x random contour. The complete pole figure is produced in Figure 2.13(c).

Apart from the above two methods some other methods are also available in the literature such as the Transmission method due to Decker et al. [13], Offset quadrant method [14], spherical specimen method due to Jetter and Borie [15] and inverse pole figure method by Harris [16].

2.2.4 Rolling Textures of f.c.c. Metals and Alloys

2.2.4.1 General Observations

A random polycrystalline metal will develop a preferred orientation or texture upon sufficient plastic deformation. The nature of the deformation texture depends essentially on the crystal structure of metal and its flow characteristics. The resulting texture may be affected to some extent by many other factors such as initial texture, the chemical composition, the previous chemical or thermal treatments, the temperature, rate or physical constraints during deformation, etc. Many theories have been put forward to date to explain the formation of texture in polycrystalline aggregates. However, the complexity of the deformation process of the individual grains in a polycrystal, particularly at large strains, and the usual complexity of the polycrystalline texture itself impose great difficulty in the derivation of a theory on rigorous grounds. As a first step towards the understanding of texture formation in polycrystals, much effort has been made in the study of texture developments in single crystals.

Pure f.c.c metals and alloys are known to exhibit three different type of rolling textures; namely (i) α - brass or alloy type texture in materials of low stacking fault energy; and (ii) copper or pure metal type texture in materials of medium stacking fault

energy; (iii) aluminum type texture in very high stacking fault energy materials [1]. A large number of investigations have been made to characterize the rolling texture of pure Cu and Al and a number of their alloys. On the basis of these results it is now known that while in α - brass or alloy type texture one has particularly only the brass (B_s) component {110} <112>, and in copper or pure metal-type the Cu {112} <111>, S {123} <634> and brass components are nearly equal strong, it is the S component which predominates in aluminum-type.

For higher Stacking Fault Energy (SFE) materials, the stacking fault width is very low, and the stacking faults are easily constricted. In that situation, the cross slip becomes easier and the material undergoes slip deformation rather than twinning. When the deformation is governed mainly by slip mode, the deformation texture is generally copper type {112} <111>. Examples, pure copper, pure nickel or nickel with low amount of cobalt, Ni-Fe alloy etc. The (111) pole figure for 95% cold rolled pure copper is shown in Figure 2.14.

Along with the copper components of texture other components like B_s component {110} <112>, S component {123} <634>, Goss component {110} <001> etc. are present in very small percentage. The materials with lower SFE predominantly exhibit B_s type of texture.

For lower SFE, the stacking fault width is much greater, which makes it difficult to create any constriction within the stacking fault region and the cross slip becomes difficult. As, a result of it, the critical resolved shear stress (CRSS) for twin becomes less than that of slip and the plastic deformation is essentially governed by the twinning process. Figure 2.15 exhibits the typical B_s type texture of a Ni-Co alloy with a lower SFE.

In Ni-Fe system if Fe content is increased, even up to 40% no significant change in SFE is observed as in Figure 2.16 and accordingly the texture is predominantly Cu type shown in Figure 2.17. But in Ni-Co system, the SFE significantly decreases on

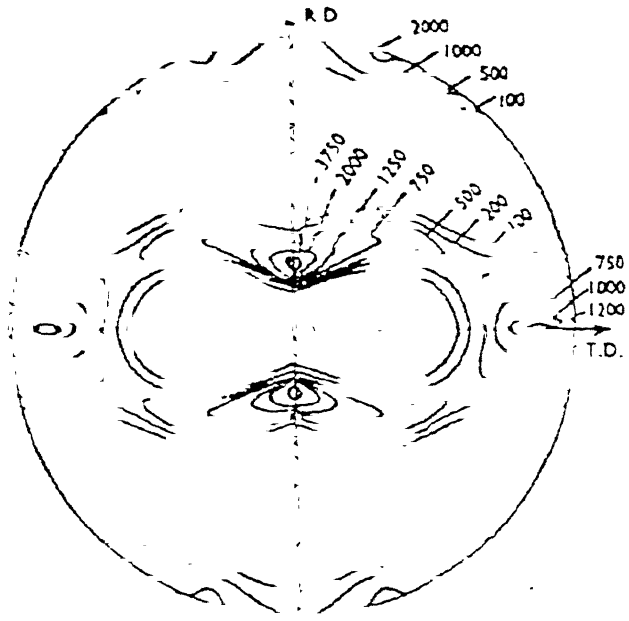

Figure 2. 14. (111) pole figure for 95% cold rolled copper [30].

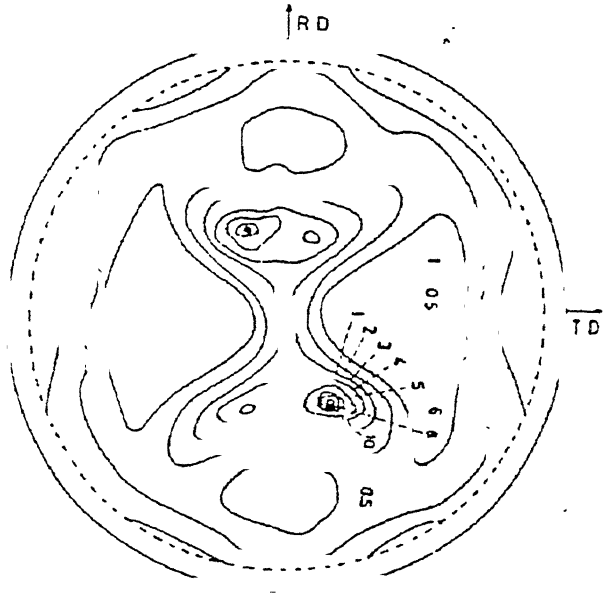

Figure 2.15. The typical B_s type deformation texture in Ni-60Co alloy [30].

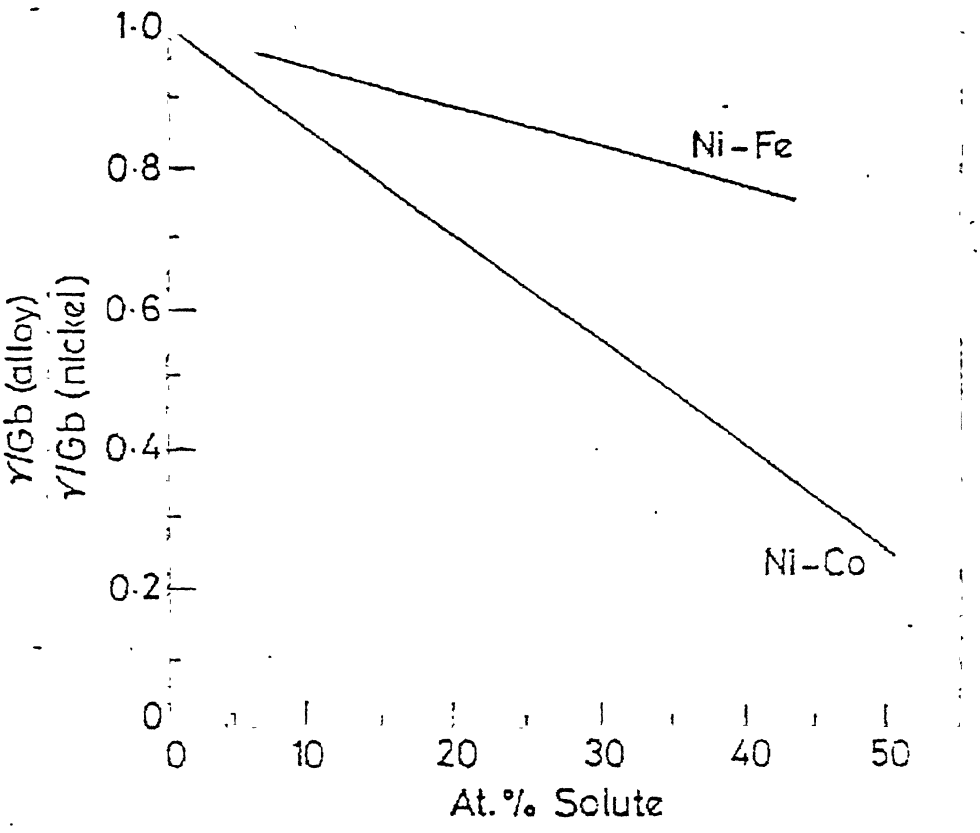

Figure 2.16. The effect of composition on stacking fault energy (SFE) [Ref: B. Bhattacharya, M. Tech Thesis, (1992), Indian Institute of Technology, Kanpur, India].

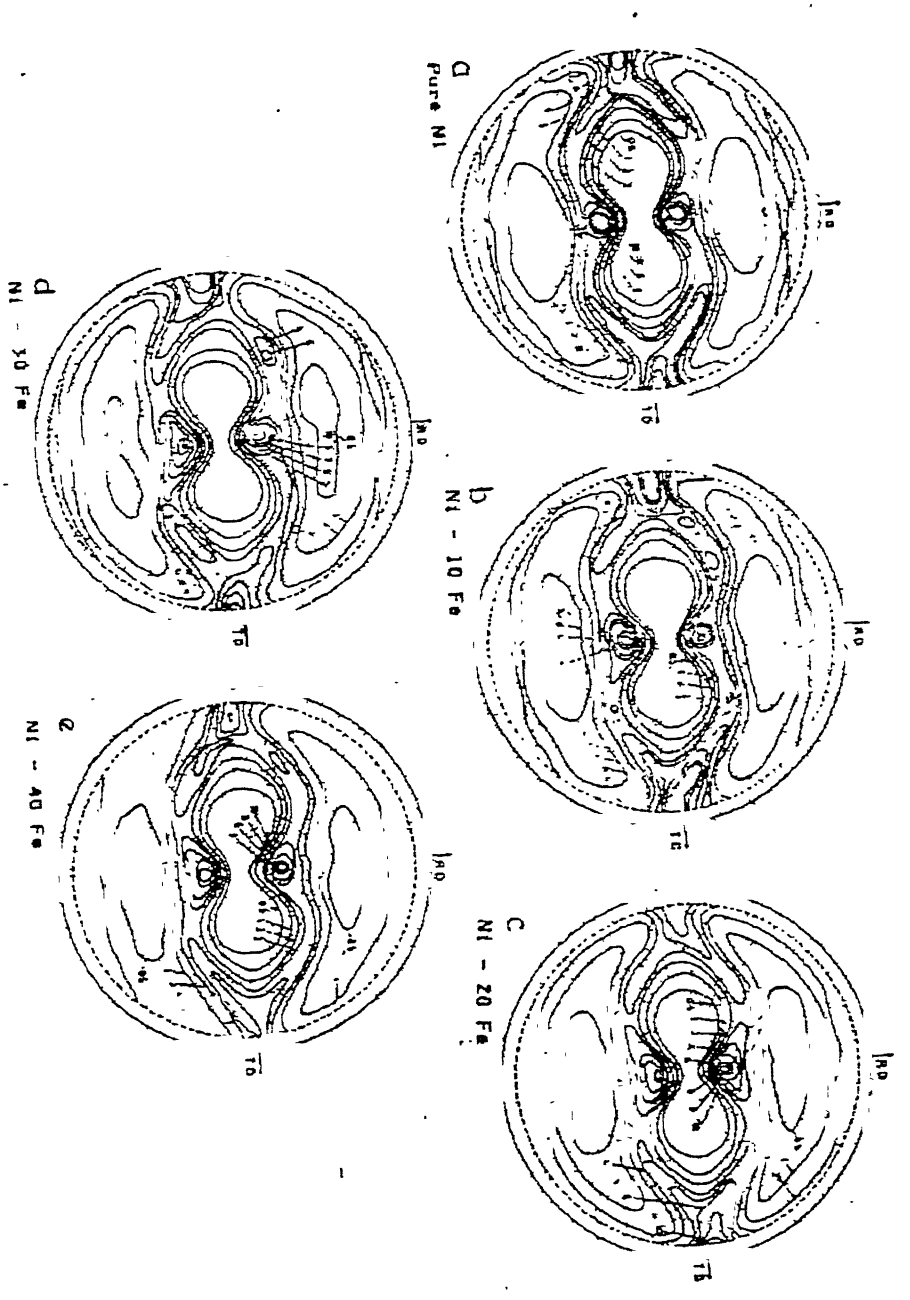

Figure 2. 17. Rolling texture of different Ni-Fe alloys [Ref: B. Bhattacharya, M. Tech Thesis, (1992), Indian Institute of Technology, Kanpur, India].

increasing the Co percentage. Accordingly it is observed that the Cu component of rolling texture gradually decreases from pure Ni to Ni-30% Co, presented in Figure 2.18. Ni-40% Co alloy shows a transition from Cu type to B_s type rolling texture, and Ni-60% Co alloy predominantly exhibits B_s type texture.

This is also observed that Cu type texture decreases with increasing amount of deformation. In case of Ni-40% Co alloy the intensity of Cu type texture remarkably decreased from 40% cold rolling to 95% cold rolling.

So it is apparent from the above discussion that there is a gradual transition of texture from pure Cu type to α – brass type depending upon the concentration of Co present which in turn regulates its stacking fault energy and this phenomenon has been described as *texture transition.*

2.2.4.2 Phenomenon of Texture Transition in Some F.C.C. Metals and alloys

The effect of solute additions on the deformation textures of a number of f.c.c metals has been investigated by Smallman [17], Liu and Richman [18] and others. Smallman showed that the texture transition from Cu to α – brass type was caused by the addition of elements like aluminum, zinc and germanium. Liu and Richman confirmed the transition for the elements phosphorous, arsenic, germanium and tin in copper. Hatherly [19] reported a similar addition to copper. Clark et al. [20] have shown that pure nickel has a texture similar to that of copper. However, a gradual transition has been found to an α – brass type texture when cobalt is added to solid solution [21].

Smallman, Liu and Richman showed that for a given solute, a minimum amount is needed to initiate texture transition and the degree of transition increases with increasing solute concentration. For complete transformation to occur a characteristic amount of solute is needed, which varies from solute to solute. Further addition of solute doesn't change the texture. Smallman [17] tried to correlate the amount of the solute required for complete transition with the atomic misfit between the solute and the solvent elements. He suggested that that for a given solvent metal, the greater the misfit of solute atoms in the solvent lattice, the lower is the concentration required to complete the texture transition. Thus, according to Smallman, elastic interaction between the solvent and solute atoms is the most important factor in determining the mode of deformation and

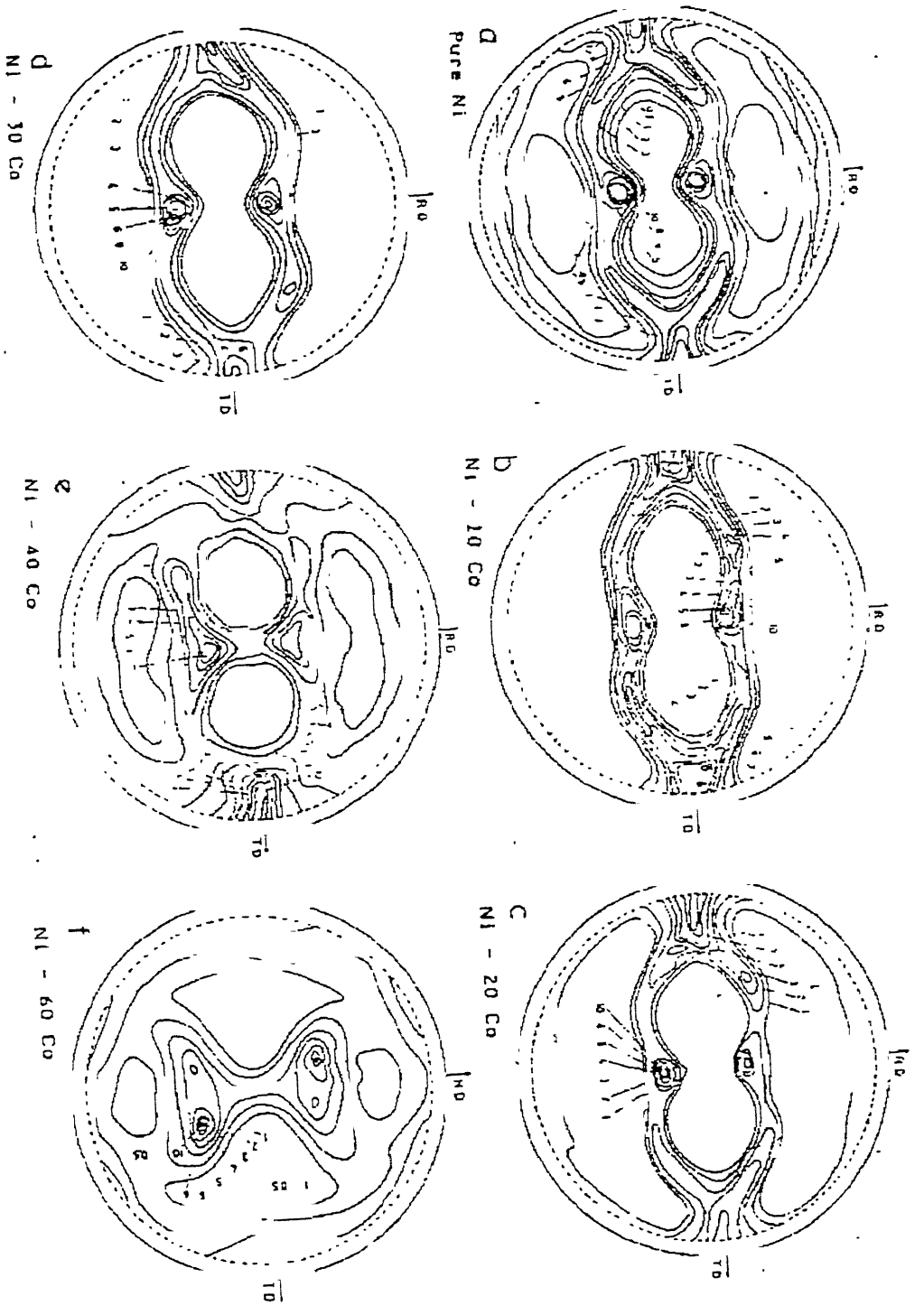

Figure 2.18. Rolling texture of different Ni-Co alloys [Ref: B. Bhattacharya, M. Tech Thesis, (1992), Indian Institute of Technology, Kanpur, India].

hence texture. Liu and Richman [18], on the other hand, suggested that the combination of electronic and ion-core interactions might be more important than elastic interaction in initiating a texture transition. A typical example of texture transition from Cu to α – brass type, on the addition of increasing amounts of zinc to copper, is shown in Figure 2.19.

In an attempt to characterize f.c.c. preferred orientation over the range from the 'pure-metal' or Cu type to the alloy or α – brass type texture, a number of attempts have been made. The parameter suggested by Smallman [17] was based on a ratio of intensities near the center of the (111) pole figure. A second parameter proposed by Liu and Richman [22] was based on the ratio of intensities on the periphery of the (111) pole figure at the transverse direction (I_{TD}) to that ~20° from the rolling direction (I_{20}). This parameter was supposed to be more sensitive than that of Smallman and was used by Dillamore et al. [23]. The texture of various f.c.c. pure metal rolled 95% at room temperature are listed in Table 2.2 with a qualitative as well as a quantitative description in terms of the parameter I_{TD}/ I_{20}. The amounts of various solute elements to bring about the complete change in texture have been cited for each element.

Hu and his co-workers [24-27] suggested a general correlation between the temperature dependence of rolling texture transition and of stacking fault frequency or probability, α, as obtained from X-ray peak shift measurements and found that the occurrence of α – brass type texture is associated with high stacking fault frequencies as opposed to Cu type which is associated with relatively low stacking fault frequencies. Smallman and Green [28] followed the transition from Cu type to the brass type texture that occurs on alloying and related this to a decrease in stacking fault energy, using copper-aluminum and copper-germanium alloys. Haessner [21,29] employed a similar correlation for the texture transition that takes place when cobalt is added to nickel.

Changing the deformation temperature can also bring about transition of rolling texture from pure-metal to alloy type [30]. Electrolytic copper when deformed at -183°C, resembles α – brass type texture. The texture of electrolytic copper rolled to –80, -140 and -196°C are shown in Figure 2.20. A comparison between Figure 2.19 and 21 clearly indicates the striking resemblance between the texture produced by increasing the alloy content and by lowering the rolling temperature.

Table 2.2. Effect of alloying on texture [35]

Metal	Texture	I_{TD}/I_{20}	At-% solute to transform to alloy texture for 95% deformation
Aluminum	"Pure-metal"	0.42	-
Copper	"Pure-metal"	0.72	20% Zn, 8% Al, 4% Ge, 3.5% Sn, 2% P, 3% As, 1.5% Sb.
Gold	"Pure-metal"	0.75	8% Zn
Lead-2% Calcium	"Pure-metal"		-
Nickel	"Pure-metal"	0.49	50% Co, 10%Mo
Palladium	"Pure-metal"	0.55	-
Platinum	Intermediate	0.94	-
Rhodium	"Pure-metal"	0.67	-
Silver	"Alloy"	1.31	-
Thorium	"Pure-metal"	~0.7	90% Ce
Ytterbium	"Alloy"	1.30	-

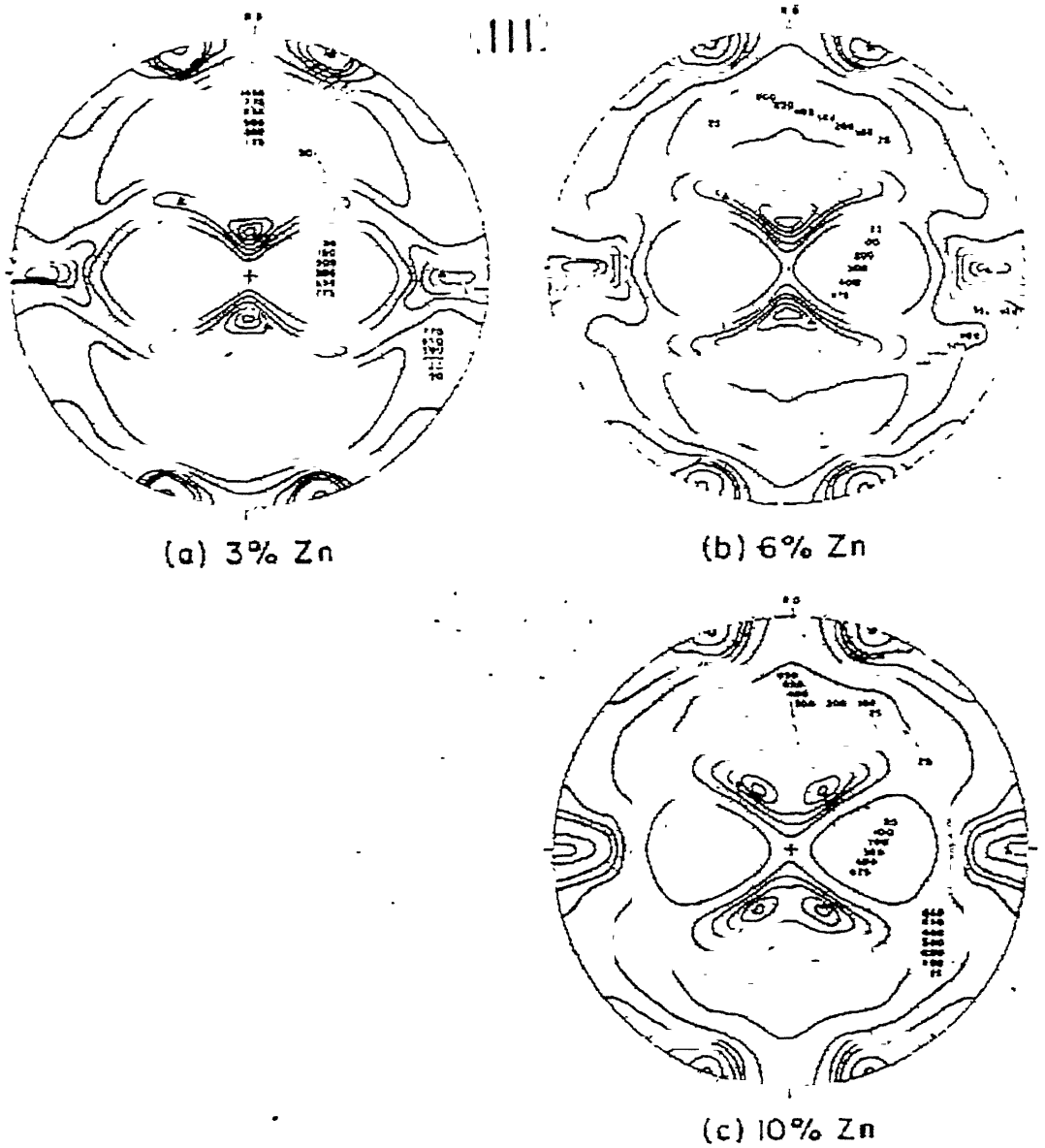

Figure 2.19. Texture transition in brass as a function of zinc content, (a) 3%, (b) 6%, (c) 10% Zn. Rolling reduction 96% [36].

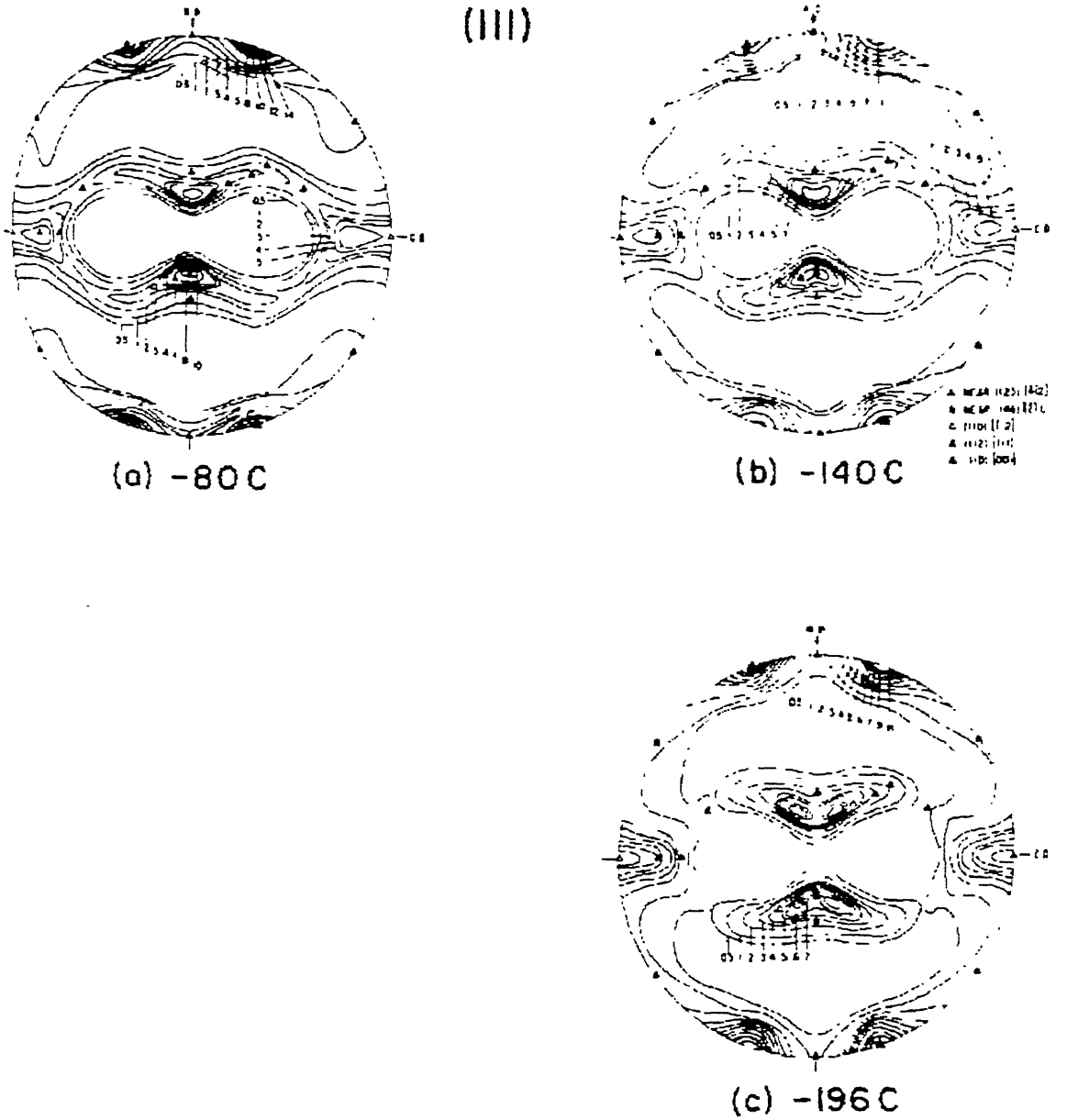

Figure 2.20. Texture transition in copper as a function of deformation temperature, (a) -80^0C, (b) -140^0C, and (c) -196^0C. Rolling reduction 96.6% [36].

The temperature dependence of texture transition was found to be very sensitive to impurity contents. As for example, no essential change in texture was observed in high-purity copper (99.99% pure) by rolling at -196°C [31]. The change in texture in 99.99% pure copper rolled at -196°C was found to be somewhat less pronounced than that found in electrolytic copper [32].

There is evidence to show that raising the temperature of deformation above room temperature can also affect texture transition. One such example is the pure metal silver. Pure silver has been found to develop a texture similar to that of α – brass when rolled at room temperature, whereas when rolled at elevated at temperature it assumes a texture similar to that of pure copper [24,25]. Smallman [17] reported that for brass containing 5% Zn, rolling at -183°C produced the usual $(110)[\bar{1}12]$ texture, whereas rolling at 200°C produced a mainly copper type texture.

2.2.5 Theories of Rolling Texture Development in F.C.C. Metals and Alloys

Barrett and Underwood [33,34] have adequately reviewed the earlier theories of deformation textures due to Wever and Schmid, Boas and Schmid, Pickus and Mathewson, Taylor, and Hibbard and Yen. The later theories have been reviewed in detail by Dillamore and Roberts [35], Hu, Cline and Goodman [36], and Haessner [37].

Of the later theories the ones by Calnan [38] and Bishop [39] were based on the idea that overshooting due to unequal hardening of primary and latent slip planes may influence the texture formation. This idea enjoyed some support, notably from Smallman [18]. A difficulty here was that silver, a pure metal not known to 'overshoot', was found to have the alloy type texture. Both Calnan [40] and Smallman [28] later rejected the theory of overshoot.

The four most recent theories of texture formation in f.c.c. metals and alloys have, in one way or the other, inherited some of the basic principles or method of analysis used in the earlier theories of deformation textures. In all four theories more or less obvious use was made of the concept of stacking fault energy in the development of textures.

Haessner [41] proposed that texture transition in f.c.c. metals and alloys is caused by non octahedral slip. According to him normal octahedral slip will lead to the $(110)[\bar{1}12]$ brass type texture. Copper type texture will be developed if slip can also occur

on the {100} planes in the <110> direction as an additional deformation mode to the {111} slip. Haessner's proposition is in line with that of Pugh [42] to explain the ideal orientation $(112)[1\bar{1}\bar{1}]$. They assumed that a second shear in the {110}<110> system following normal octahedral slip would change the $(110)[\bar{1}12]$ orientation into $(112)[1\bar{1}\bar{1}]$. It was further proposed by Haessner that for metals with low stacking fault energy, cubic slip would become more difficult as the separation of partials in the {111} plane becomes wider.

A theory based on dislocation interaction has been proposed by Liu [43] to explain the formation of rolling texture in f.c.c. metals and alloys. He considered that during deformation the slip systems which operate are determined by the ability of dislocations on these slip systems to interact producing a net reduction in energy. Having determined which sets of four slip systems give the greatest reduction in energy, the end texture is the orientation at which the slip rotations on the operating systems cancel out. On this basis Liu predicted that for metals of low stacking fault energy the ideal orientations were $(110)[\bar{1}12]$ plus an orientation spread with (110) rolling plane. The ideal end orientation for metals of relatively high stacking fault energy was shown to be close with $(358)[52\bar{3}]$.

Hu et al. [36] pointed out that although these results were in essential agreement with the two types of rolling texture observed in f.c.c. metals and alloys, the $(112)[1\bar{1}\bar{1}]$ orientation of the copper type texture was not predicted from Liu's analysis. This theory has also been argued on the basis that there would, in reality, be not reduction in internal energy due to the interaction of dislocations on the operating systems. The main drawback with Liu's theory is that it is highly hypothetical in nature and little experimental verification has been made possible.

Dillamore and Roberts [44] proposed their 'cross slip' hypothesis in order to explain the deformation texture in f.c.c. metals and alloys. They suggested that all f.c.c. metals and alloys first develop $(110)[\bar{1}12]$ or the brass type texture by normal slip. The copper-type pure metal texture is developed if, in addition to {111} slip on the primary and secondary slip systems, larger amounts cross slip also takes palce on the other planes. Dillamore and Roberts determined the end point of rotation for all possible initial grain

orientations and found that, while most orientations rotate to {110}<112>, some move initially to {110}<001>. Following the principles of stability proposed by Tucker [45], these two workers considered the stability of the various multiple slip orientations and concluded that {110}<112> is the only true stable orientation under "normal" slip processes. For metals of low stacking fault energy, cross slip is difficult and plastic deformation occurs largely by normal slip. Hence the final texture remains as $(110)[\bar{1}12]$ or the brass type. For metals with high stacking fault energy, cross slip is easier and the normal $(110)[\bar{1}12]$ slip texture will undergo further reorientation by cross slip to assume the copper-type pure metal texture. Since the stacking fault energy of a metal decreases with increasing alloy addition, and since cross slip can be activated by thermal fluctuations, the 'cross slip' hypothesis, therefore, appears to be consistent with both the composition and temperature dependence of texture transition in f.c.c. metals and alloys. It is also interesting to note that on the basis of their hypothesis, these two workers were able to predict a pole figure which fits the difference between copper and aluminum type texture.

A strong objection to the cross slip hypothesis was put forward by Haessner [37]. He pointed out that the internal stress attained in rolling is largely independent of the stacking fault energy of the material and is much higher than the stress at which cross slip starts to occur in single crystals at 0°K. Haessner [37] concluded that cross slip should always be possible during the rolling of polycrystalline metals and so this phenomenon could not be the fundamental reason for the existence of the two types of rolling texture in f.c.c. metals and alloys. There is experimental evidence of cross slip in α – brass at room temperature, and also in copper at very low temperatures. Although these observations appear to rule over the cross slip hypothesis, Dillamore and Roberts [35] have suggested that very large amounts of cross slip necessary to modify the rolling texture may only occur when the stacking fault energy is high.

Geometrically, equal proportions of slip on two {111} planes, namely, the primary and the cross slip plane is equivalent to cubic slip. Thus the theories of Haessner and Dillamore and Roberts lead to the same model that is capable of explaining the textures in f.c.c. metals and alloys.

The 'twin hypothesis' put forward by Wassermann [46] is quite different from the three slip theories already discussed. According to him mechanical twinning is supposed to be responsible for the observed texture transition in f.c.c. metals and alloys. He assumed that, during deformation, all metals tend to develop the copper-type pure-metal texture by means of slip on {111} planes. For the development of the α – brass type texture, mechanical twinning, as an additional deformation mode, is essential. He proposed that the rolling texture of f.c.c. metals and alloys can be considered as being composed of two limited fiber texture centered on the orientations {110}<112> and {112}<111>. If mechanical twinning in the systems {111}<211> is considered as a possible deformation mode in addition to normal slip, then the material in the {112}<111> orientation may be transformed by twinning to the {552}<115> orientation as in Figure 2.21, which rotates into the {110}<001> orientation by subsequent slip. Wasserman argued that the {110}<112> orientation does not change during deformation, because twinning of the orientation would lead to shape change that do not meet the strain requirements of the rolling process. The proposed mechanism is in agreement with the observation that metals of low stacking fault energy may deform by mechanical twinning [47] and it is in that metals which exhibit the alloy texture. The theory is also consistent with the observations on the temperature dependence of twinning in f.c.c. single crystals.

Kallend and Davies [48] performed a computer simulation of the development of rolling texture in f.c.c. metals and alloys assuming that the deformation mode is multiple {111}<110> slip. The predicted crystallite orientation distribution function for 40% and 80% reduction was found in good agreement with the experimentally determined texture of cold rolled copper. They also noticed that if deformation twinning is included as an additional deformation mode, following a simple strain accommodation criterion for twinning, a satisfactory agreement with the experimentally determined texture of cold-rolled copper –10% Zn (which shows the alloy texture) is obtained.

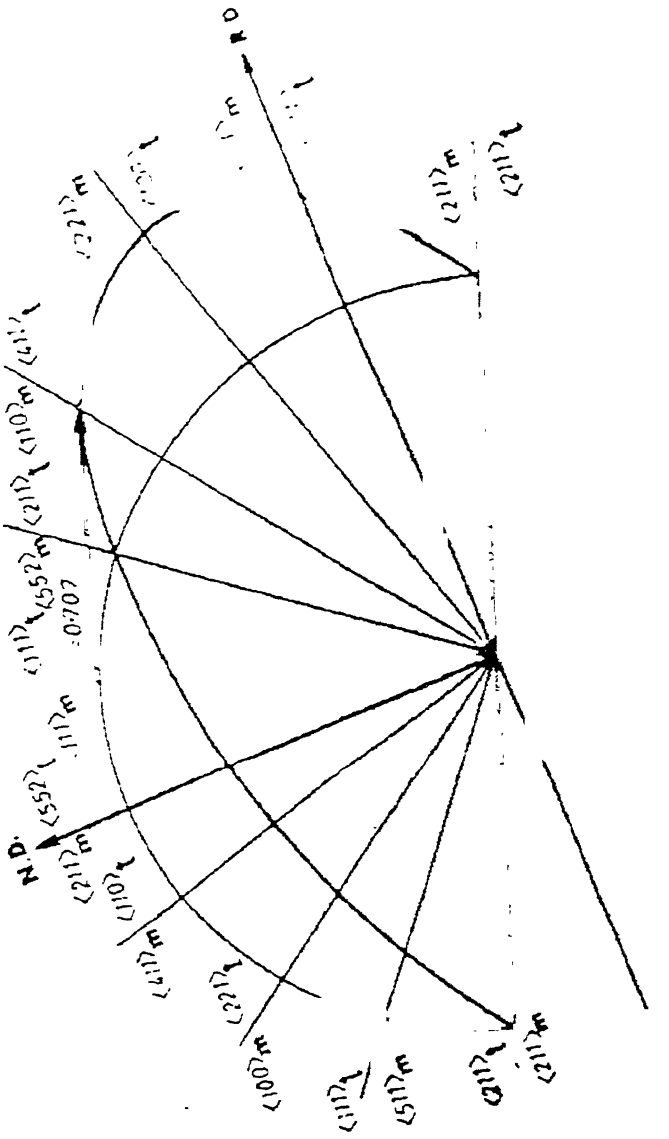

Figure 2.21 Diagram illustrating the relationship between {112} and <111> orientation matrix and its twin orientation formed under the stress system operative during rolling, showing that the direction of maximum extension is close to the rolling direction (R.D.) and that of minimum extension is close to the sheet normal (N.D.). Suffixes m and t denotes matrix and twin directions, respectively [46].

2.3 Objective of the Present Work

It appears from the foregoing discussion that Ni-Co system in particular constitute a very important alloy system, from the point of view that the stacking fault energy varies with increased cobalt addition. Stacking fault energy is found to have a great bearing in the deformation texture of f.c.c. metals and alloys, particularly the transition of texture from copper-type to α-brass type. There is considerable dispute among previous workers regarding the actual process that causes the deformation texture of low stacking fault energy f.c.c. alloys to transform from pure metal type to alloy type. So a detailed study of the deformation texture in Ni-Co system will give a deep insight into the actual mechanism of texture transition in f.c.c. metals and alloys. This work was undertaken to throw some light on this aspect.

CHAPTER 3
EXPERIMENTAL PROCEDURE

3.1 Material and Initial Treatment

The chemical compositions of the alloys used in the present study are given in Table 3.1. Both nominal and detailed compositions of each alloy are shown in the table. All the alloys were induction melted. Segregation was avoided by magnetic stirring during melting. Subsequently they were cast under an protective argon atmosphere The ingots were cold-rolled 50% to a thickness of 6 mm and then homogenization annealed in vacuum at 820^0C for 3h. These were then again cold-rolled 50% and annealed at 820^0C for a period of 3 h to yield the starting material of almost random texture.

The starting materials were cold rolled to 20% and 35% reductions, using a laboratory rolling mill having 250 mm diameter rolls.

3.2 Optical Microscopy

After cold rolling, the small pieces of all the materials were mounted within cold setting resin, for optical microscopy purpose. After mounting, these samples were subjected to conventional metallographic polishing and then etching. The etching reagent was prepared by mixing 50% (by volume) conc. HNO_3 with 50% (by volume) glacial acetic acid. Sometimes, a few drops of hydrofluoric acid were added for better and instant effect. To get the best effect, always freshly prepared etching reagent was used.

The etched samples were examined under an optical microscope, and photographs of each sample were taken.

3.3 Electron Microscopy

Cold-rolled sheets of sizes of sizes ($20\times20\,mm^2$) from all three alloys were initially thinned down by mechanical polishing using emery paper of 1/0 grade. Afterwards, they were thinned down by chemical polishing using a solution containing HNO_3 and HF. Then 3mm.diameter disk was cut out from them using a manual disk-puncturing machine. These were then further thinned down for electron transparency using a twin-jet electro-polishing unit. The usual voltage used for thinning was between 30 to 35 volts. A

Table 3.1 Chemical compositions of alloys in the present study (wt%)

	Alloy Nominal Composition	Detailed composition						
		Fe	Co	C	S	Si	Cu	Ni
A	Ni-30%Co	-	30.90	0.006	0.003	0.03	0.03	Bal.
B	Ni-40%Co	-	41.05	0.006	0.004	0.03	0.03	Bal.
C	Ni-60%Co	-	60.50	0.006	0.004	0.06	0.03	Bal.

mixture of Ethylene glycol and water was used as the coolant. The chemical composition of the electrolyte used is given in Table 3.2. All TEM work was carried out in a JEOL JEM-2000FX microscope operating at 160 kV.

3.4 Determination and Representation of Texture

The samples used for textural measurement were electropolished using the same electrolyte used for electron microscopy and already given in Table 3.2. Texture measurement was done analyzing the Kikuchi patterns formed by back scattered electrons in a fully computer controlled SEM (Scanning Electron Microscope) for automated crystal orientation mapping. Figure 3.1 shows a schematic view of the instrument used for this purpose. The Kikuchi patterns were taken from a large no. of closely spaced points in the sample. The Kikuchi patterns thus obtained are automatically compared with those kept in the memory of the computer and automatically indexed. The ODFs are subsequently generated by the computer transforming these dataset into three dimensional orientation space defined by the Euler's angle φ, φ_1 and φ_2 using the series expansion method of Bunge [9, 49-50].

Table 3.2. Chemical composition of the electrolyte used in twin-jet polisher

Compound	Volume (%)
Ethyl alcohol	70
Ethyl mono butyl ether	10
Perchloric acid	8
Water	12

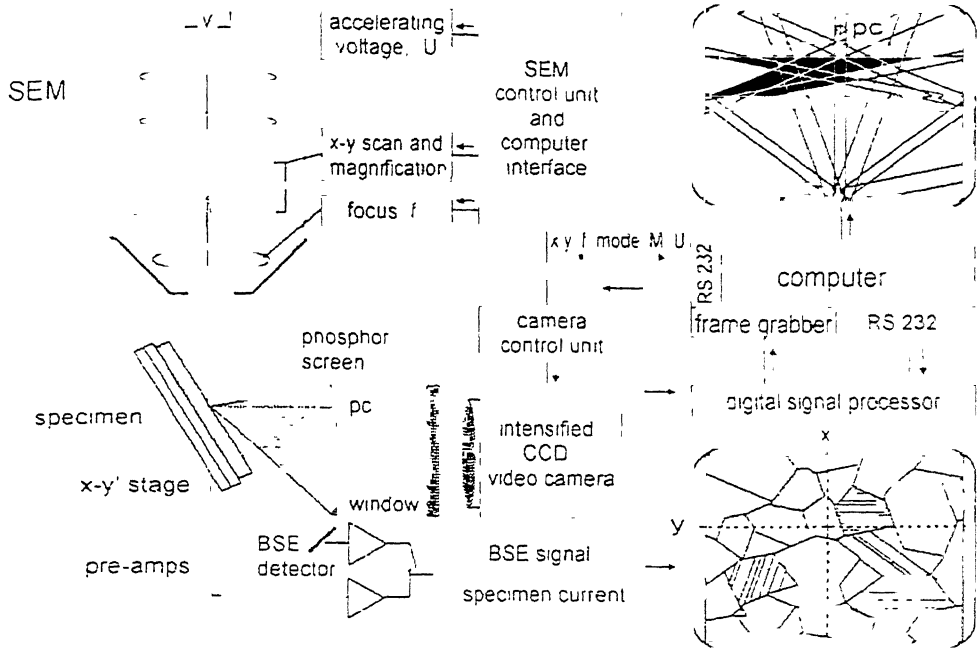

Figure 3.1 Fully Computer controlled SEM for automated crystal orientation mapping[Ref: R.A. Schwarzer, *Micron*, v. 28, n. 23, 256, (1997), Elsevier Science Ltd., UK].

CHAPTER – 4
RESULTS

4.1 Optical Micrographs

4.1.1 Starting Materials

Optical micrographs of all the samples have been analyzed at 200X magnification and the micrographs have been given in Figure 4.1.1.1 to Figure 4.1.1.9. Starting material of Ni-30Co shows distinct grain boundaries and presence of a few annealing twins (Figure 4.1.1.1) at The grains are polygonal in nature. In case of Ni-40Co also annealing twins were observed (Figure 4.1..1.2). In Ni-60Co alloy annealing twins were not revealed for starting material in optical micrographs as opposed to Ni-40Co and Ni-30Co starting material (Figure 4.1.1.3).

4.1.2 20% Deformed materials

Ni-30Co samples shows elongated grains at 20% rolling reduction in thickness in the direction of working (Figure 4.1.2.1). Ni-40Co in 20% deformed condition revealed pronounced annealing twins (Figure 4.1.2.2). Ni-60Co in 20% deformed condition also reveals some annealing twins (Figure 4.1.2.3).

4.1.3 35% Deformed Materials

Ni-30Co samples in 35% deformed condition reveals very elongated grains in the direction of working and not much twins are observed at this stage (Figure 4.1.3.1). Distinct annealing twins through the grain is observed in Ni-40Co samples in 35% deformed condition (Figure 4.1.3.2). Ni-60Co samples at 35% deformation stage shows very pronounced grain elongation effect due to rolling reduction (Figure 4.1.3.3).

4.2 Electron Microscopy

4.2.1 Starting Materials

TEM micrographs (Figure 4.2.1.1 (a) and (b)) of the starting annealed material for the Ni-30Co alloy shows typically large grains, with some dislocations inside. There are a large number of bend contours also.

Twins, sometimes quite large are an integral part of the microstructure of the starting material in the Ni-40Co alloys (Figure 4.2.1.2).

Figure 4.1.1.1 Optical micrograph of Ni-30Co starting material.

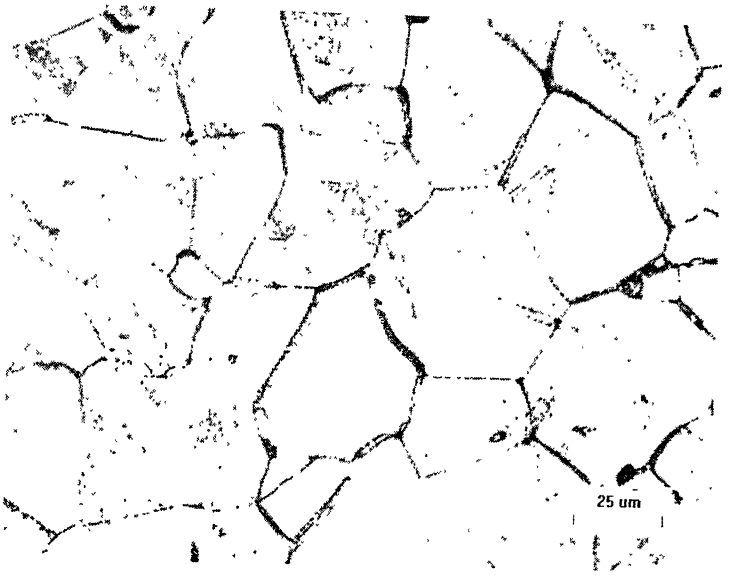

Figure 4.1.1.2 Optical micrograph of Ni-40Co starting material.

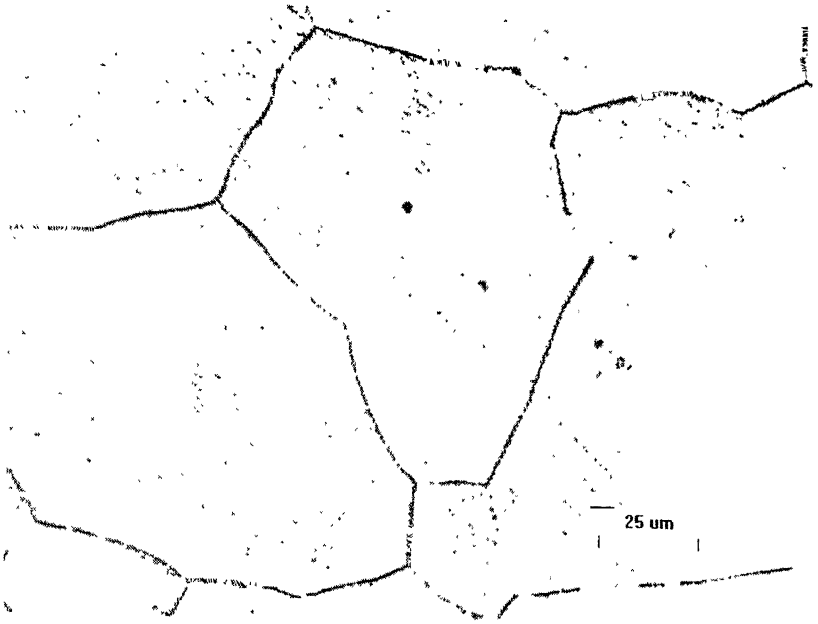

Figure 4.1.1.3 Optical micrograph of Ni-60Co starting material.

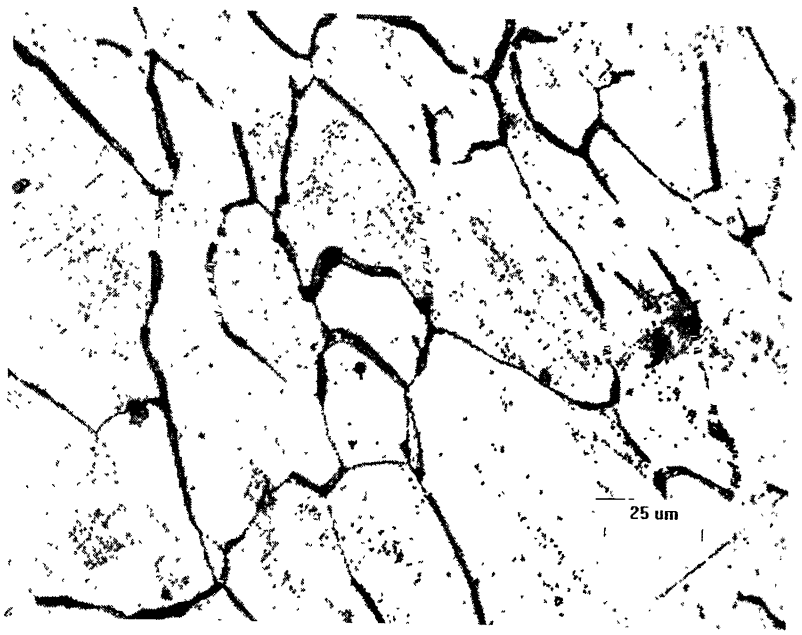

Figure 4.1.2.1 Optical micrograph of Ni-30Co in 20% deformed condition showing elongated grains.

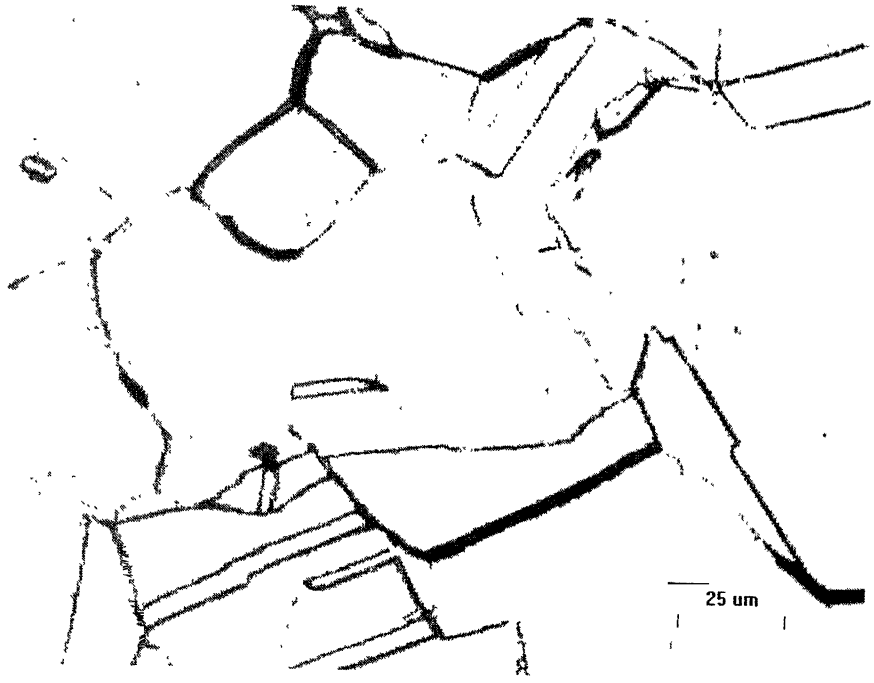

Figure 4.1.2.2 Optical micrograph of Ni-40Co in 20% deformed condition showing presence of annealing twins

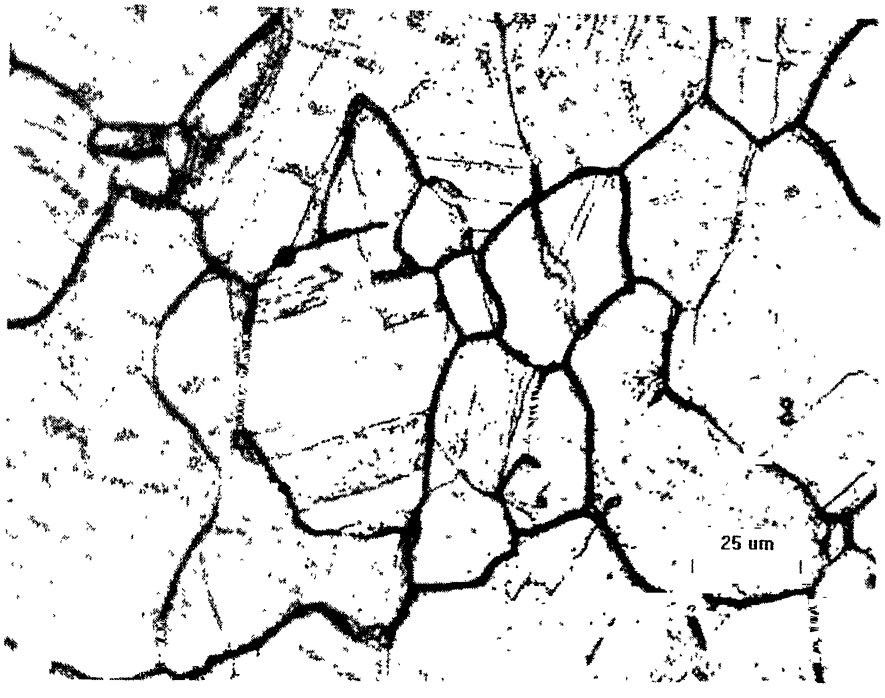

Figure 4.1.2.3 Optical micrograph of Ni-60Co in 20% deformed condition.

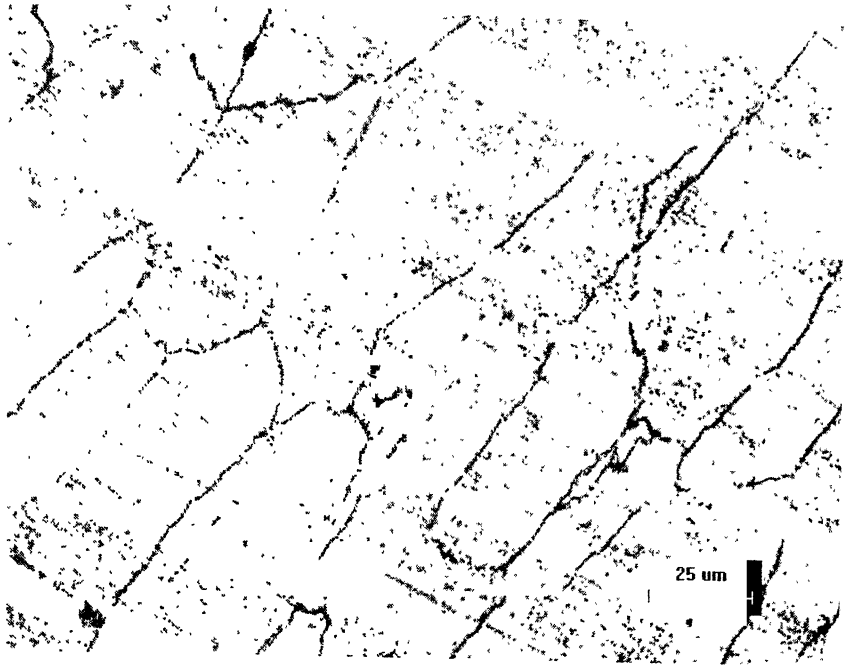

Figure 4.1.3.1 Optical micrograph of Ni-30Co in 35% deformed condition showing Elongated Grains

Figure 4.1.3.2 Optical micrograph of Ni-40Co in 35% deformed condition.

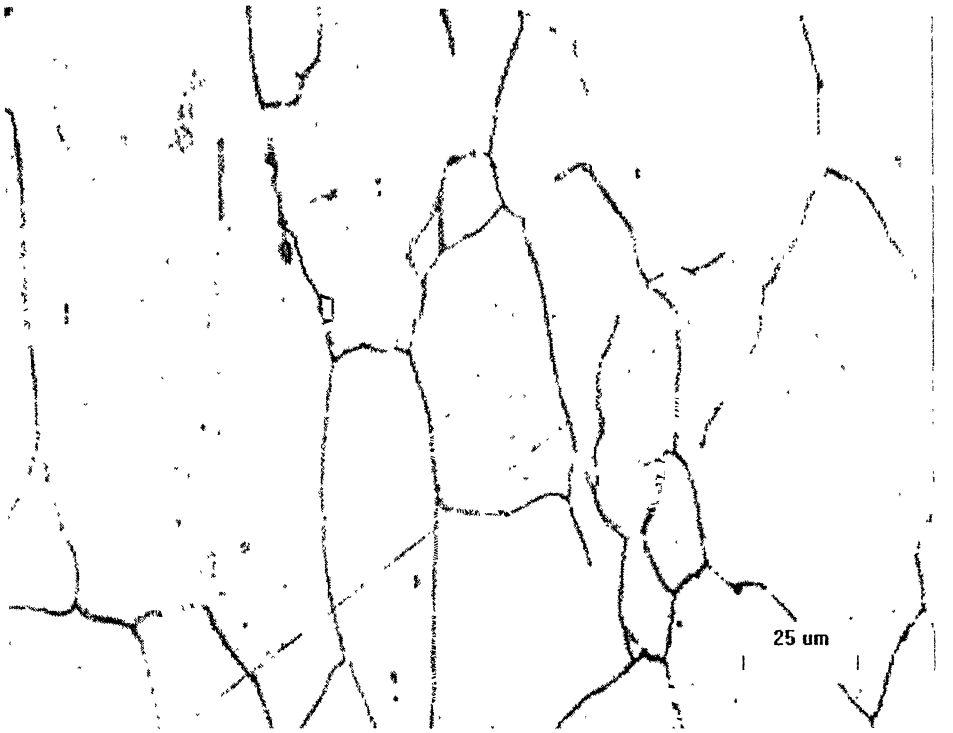

Figure 4.1.3.3 Optical micrograph of Ni-60Co in 35% deformed condition showing elongated grains.

(a) BF X 36K

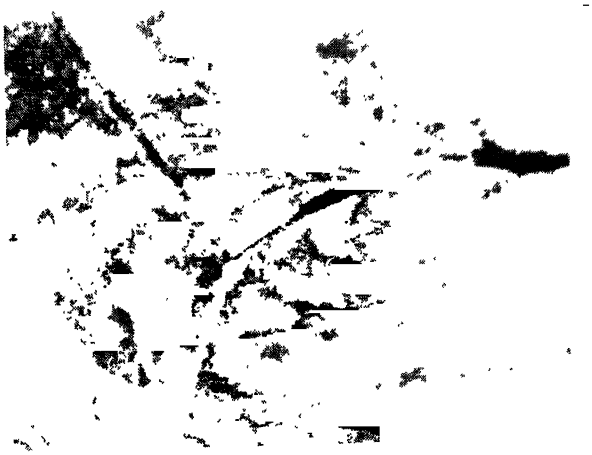

(b) BF X 15K

Figure 4.2.1.1 TEM micrograph of Ni-30Co starting material

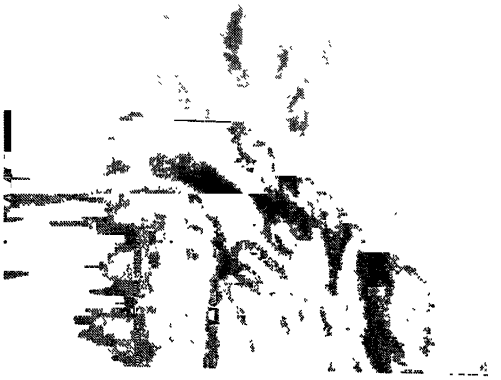

(a) BF X 30K

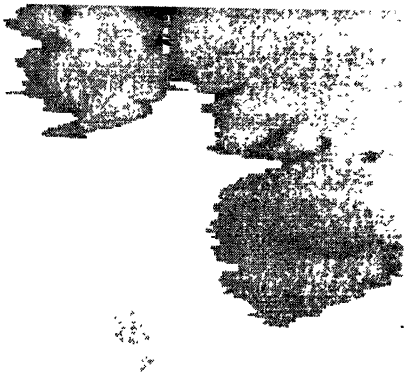

(b) BF X 30K

Figure 4.2.1.2 TEM micrograph of Ni-40Co starting material

High density of large annealing twins within grains is observed in case of the starting material of Ni-60Co alloy.

4.2.2 20% Deformed Material

- Ni-30Co alloy

  Typical TEM micrographs of the 20%deformed Ni-30Co alloy are shown in Figure 4.2.2.1 (a) and (c) along with their SADPs. The foil plane has been identified in each case at the {110}. Some extra spots can be seen in the above two SADPs which might have come from twins also. But this could not be verified.

- Ni-40Co alloy

  A typical area of the Ni-40Co alloy is shown in Figure 4.2.2.2(a) along with the SADPs from the location A and B. The foil planes were identified as {110} and {122} on the locations A and B respectively.

- Ni-60Co alloy

  A typical TEM micrograph from the Ni-60Co alloy showing microbrands is presented in Figure 4.2.2.3(a). The SADPs from the different band elements show that the first plane in each case is {112} type, only rotated from place to place by rotation around the <112> direction. Another foil from the same material shows some banded features with dislocations (Figure 4.2.2.4(a)). The foil plane from all the three plane have been identified, from the respective SADPs, as {110}. In fact the spot patterns are slightly rotated from one another by small rotations around <110> direction. The boundaries between A,B and C could thus be low angle boundaries.

4.2.3 35% Deformed Material

- Ni-30Co alloy

  The typical areas from thin foils of the 35% deformed Ni-30Co alloy are shown in Figure 4.2.3.1 along with their SADPs. While the SADP of the Figure 4.2.3.1(a) shows the {110} pattern with extra spots, presumably

(a) BF X 100K

(b) BF X 36K

Figure 4.2.1.3 TEM micrograph of Ni-60Co starting material

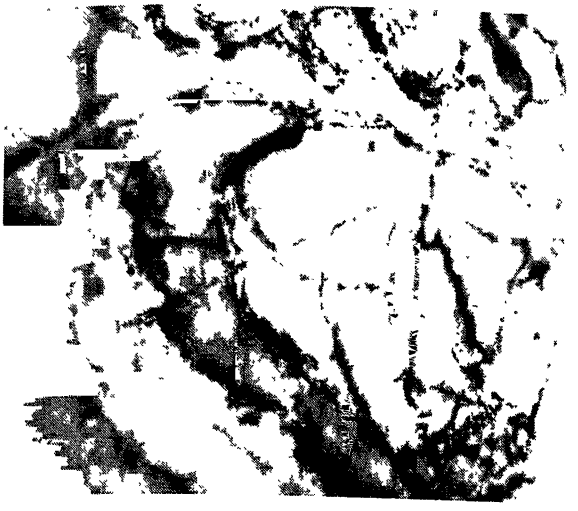

(a) BF X 150K

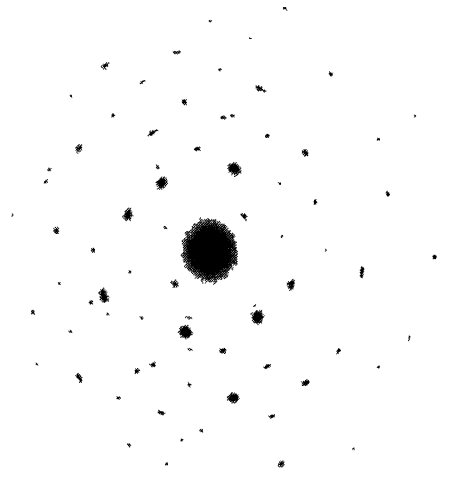

(b) SADP of whole (a) [{110} pattern]

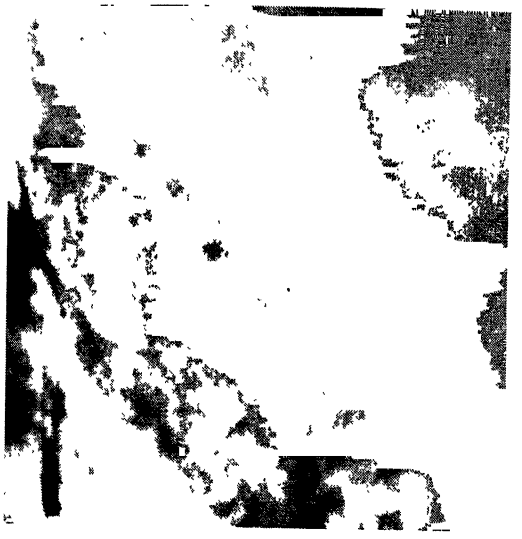

(c) BF X 100K

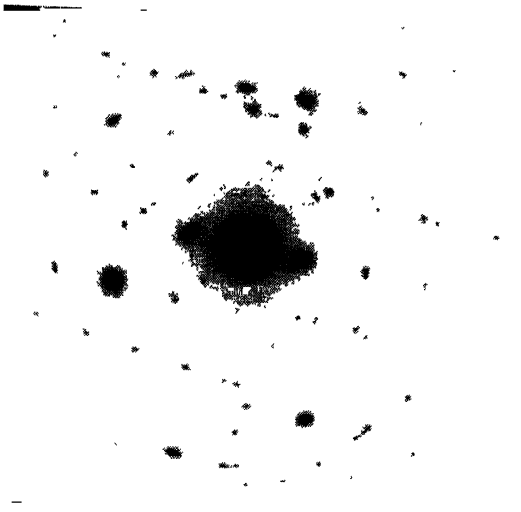

(d) SADP of whole (c) [{110} pattern]

Figure 4.2.2.1 TEM micrograph of Ni-30Co in 20% deformed condition

(a) BF X 45K

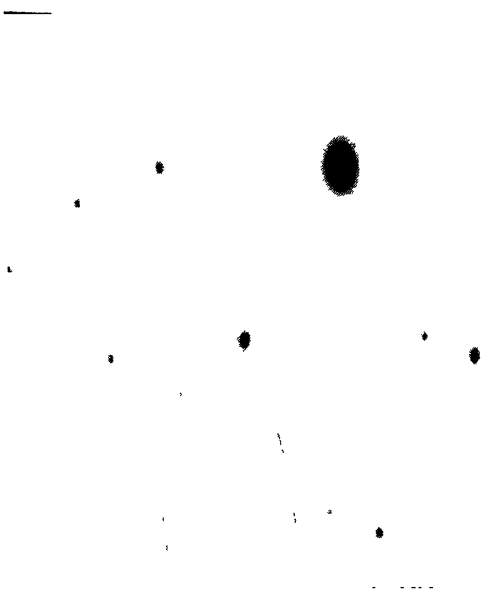

(b) SADP of area 'A' [{110} pattern]

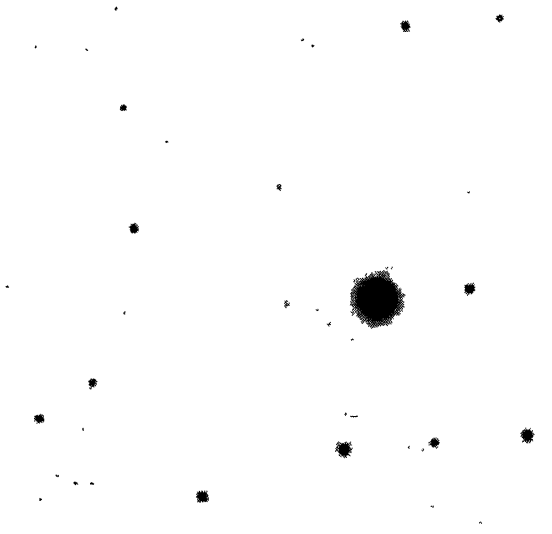

(c) SADP of area 'B' [{122} pattern]

Figure 4.2.2.2 TEM micrograph of Ni-40Co in 20% deformed condition

(a) BF X 45K

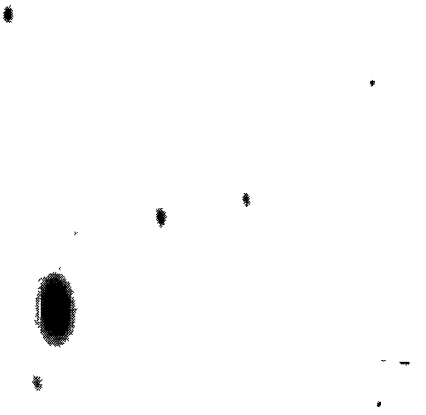

(b) SADP of area 'A' [{112} pattern

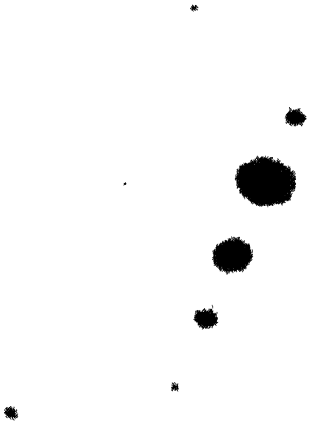

(c) SADP of area 'B' [{112 pattern]

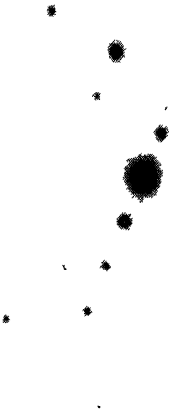

(d) SADP of area 'C' [{112} pattern]

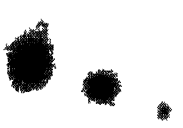

(e) SADP of area 'D' [{112} pattern]

Figure 4.2.2.3 TEM micrograph of Ni-60Co in 20% deformed condition

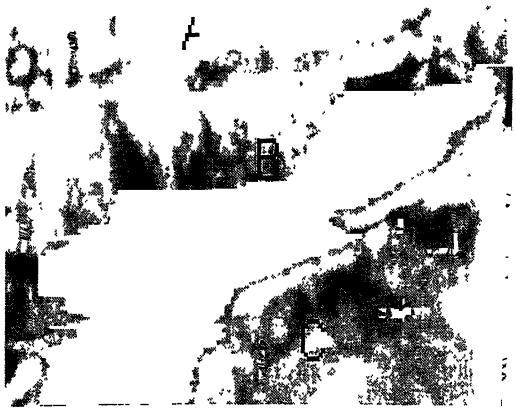

(a) BF X 36K

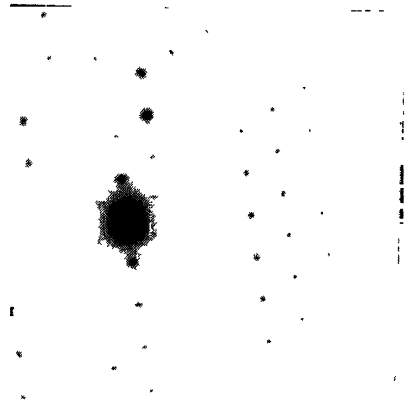

(b) SADP of area 'A'
[{1110} pattern}]

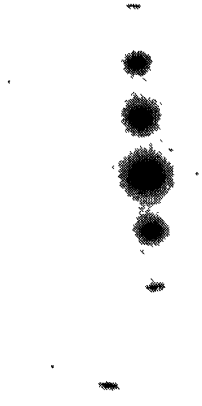

(a) SADP of area 'B'
[{110} pattern]

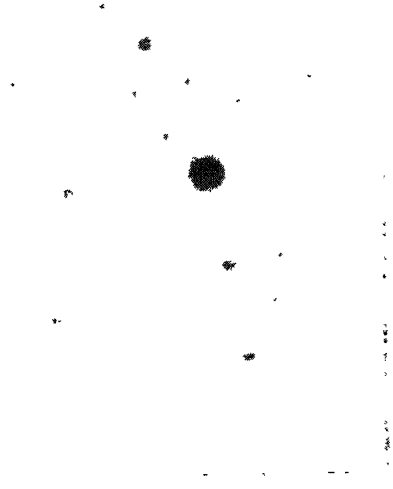

(d) SADP of area 'C'
[{110} pattern]

Figure 4.2.2.4 TEM micrograph of Ni-60C0 sample in 20% deformed condition

(a) BF X 100K

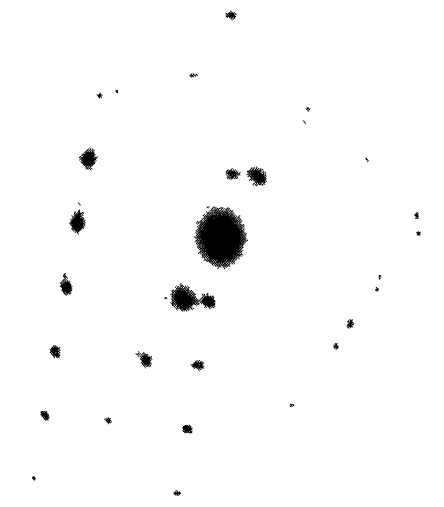

(b) SADP of whole (a) [{110} pattern with extra twin spots]

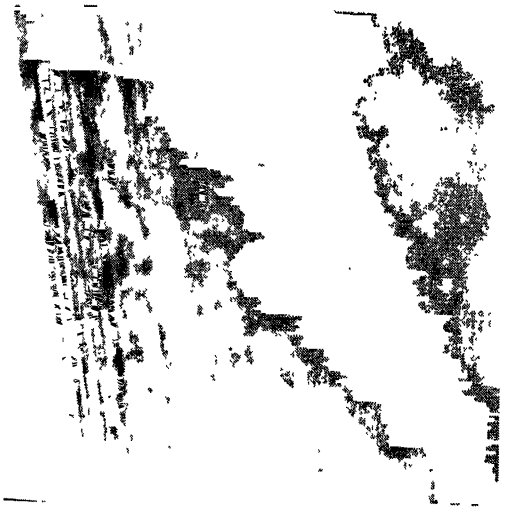

(c) BF X 200K

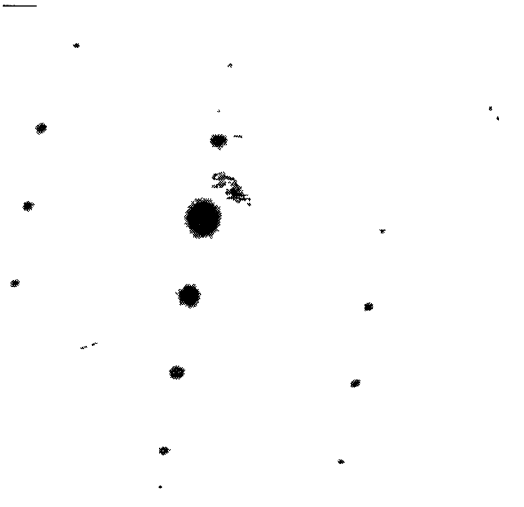

(d) SADP of whole (c) [{123} pattern]

Figure 4.2.3.1 TEM micrograph of Ni-30Co in 35% deformed condition

from twins, the SADP from the 4.2.3.1(c) shows the {123} pattern. No attempt was made to identify the twin plane here.

- Ni-60Co alloy

  The 35% deformed material from the Ni-60Co alloy shows plenty of deformation twins. Normally these deformation twins are observed in bundles. Areas with deformation twins are shown typically in Figure 4.2.3.2(a). The SADPs from different areas of Figure 4.2.3.2(a) are shown in Figure 4.2.3.2(b) to (e). The SADPs of all the four areas confirm that the foil plane is {110} in each case. The SADPs from area C of Figure 4.2.3.2(a) has been carefully analyzed and the twin spots were identified. From this the twin axis has been found out to be $[1\bar{1}1]$. An ideal SADP from a twin in f.c.c. materials is shown in Appendix A2 for comparison.

  Figure 4.2.3.3(a) again shows a large bundle of thin deformation twins in this material.

  A third typical micrograph from the same alloy shows a bundle of deformation twins extended over a large region (Figure 4.2.3.4(a)). Again the twin axis has been identified as $[1\bar{1}1]$.

4.3 Crystallographic Texture

The ODFs of all the three alloys under current investigation, at different stages of deformation, have been given in Figure 4.3.1.1, Figure 4.3.2.1 and Figure 4.3.3.1. The pole densities in the ODFs have been represented using different color codes. The locations of the Cu component and the B_S component have been marked in all the ODFs using different Symbols (□ for Cu component and + for brass component.)

4.3.1 Starting Material

The starting material for all the three alloys show rather uniform pole densities through out the Euler space (Figure 4.3.1.1). No distinct texture component can be observed in the ODF. In a way therefore the starting material can be considered as textureless. In particular, the pole densities at the exact Cu and B_S locations are practically zero in all these three ODFs.

(a) BF X 30K

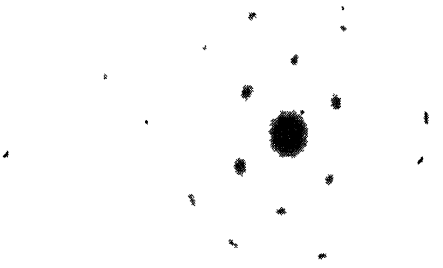

(b) SADP of area 'A' [{110} pattern]

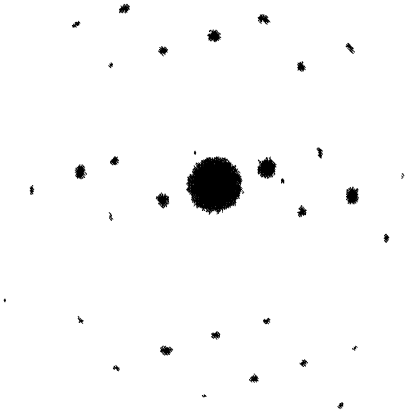

(c) SADP of area 'B' [{110} pattern]

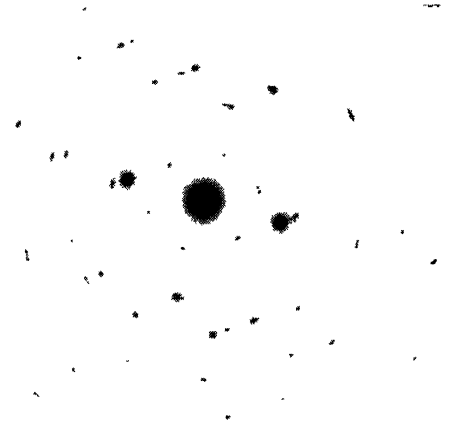

(d) SADP of area 'C' [{110} pattern]

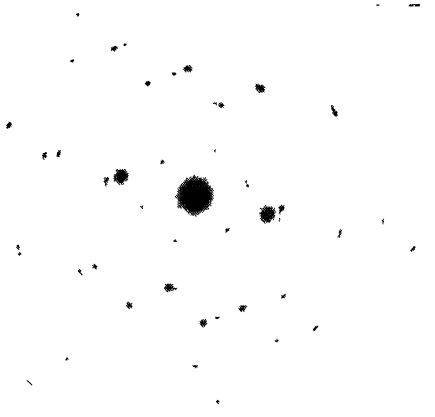

(e) SADP of area 'D'

Figure 4.2.3.2 TEM micrograph of Ni-60Co in 35% deformed condition

(a) BF X 45K

(b) SADP of area 'A'

(c) SADP of area 'B'

Figure 4.2.3.3 TEM micrograph of Ni-60Co in 35% deformed condition

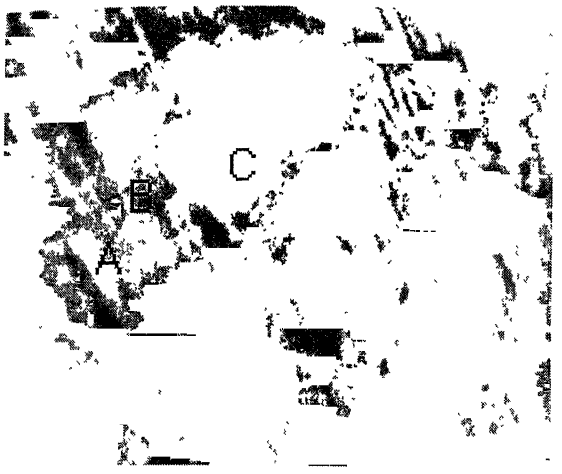

(a) BF X 60K

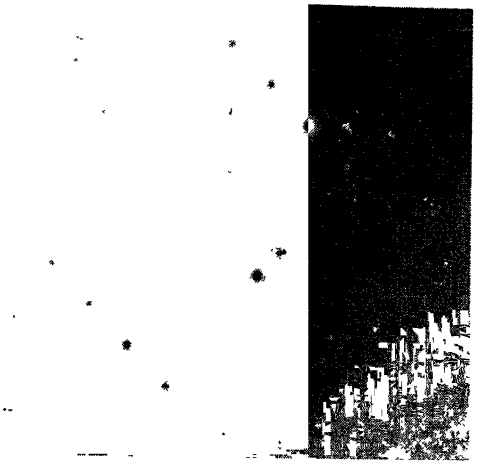

(b) SADP of area 'A' in figure (a) [{110} pattern]

(c) SADP of area 'B' in figure (a) [{110} pattern with extra twin spot, twin axis is $[1\bar{1}1]$

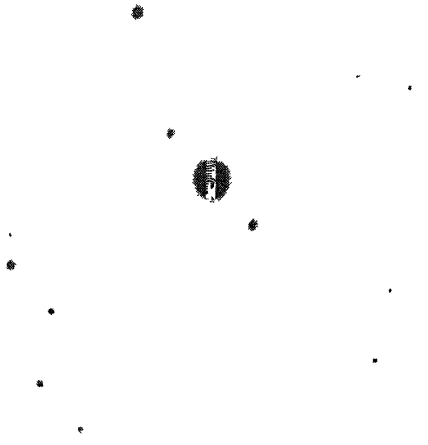

(d) SADP of area 'C' [{110} pattern]

Figure 4.2.3.4 TEM micrograph of Ni-60Co in 35% deformed condition

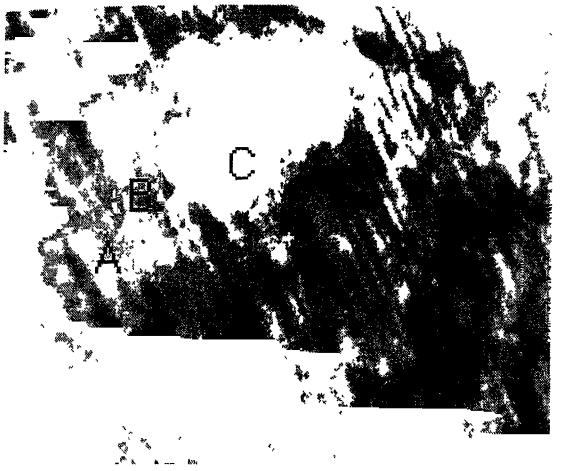

(a) BF X 60K

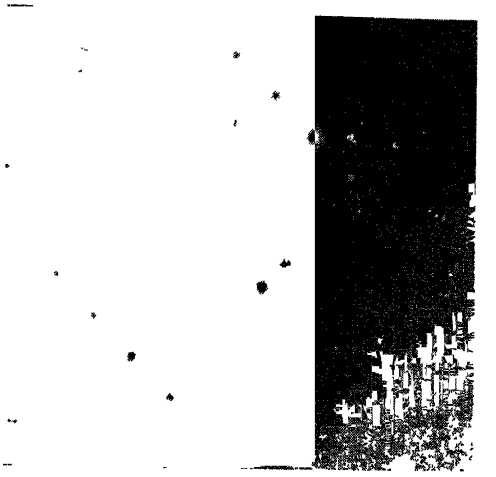

(b) SADP of area 'A' in figure (a) [{110} pattern]

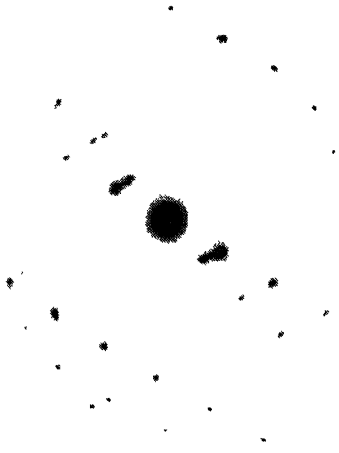

(c) SADP of area 'B' in figure (a) [{110} pattern with extra twin spot, twin axis is $[1\bar{1}1]$

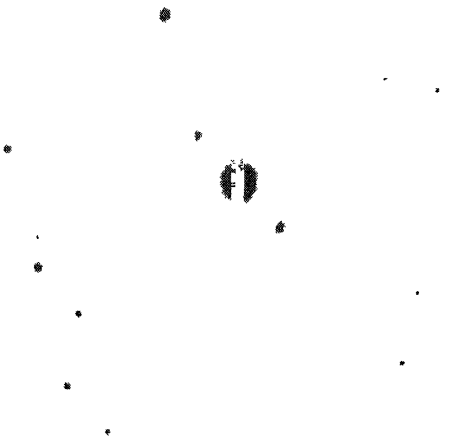

(d) SADP of area 'C' [{110} pattern]

Figure 4.2.3.4 TEM micrograph of Ni-60Co in 35% deformed condition

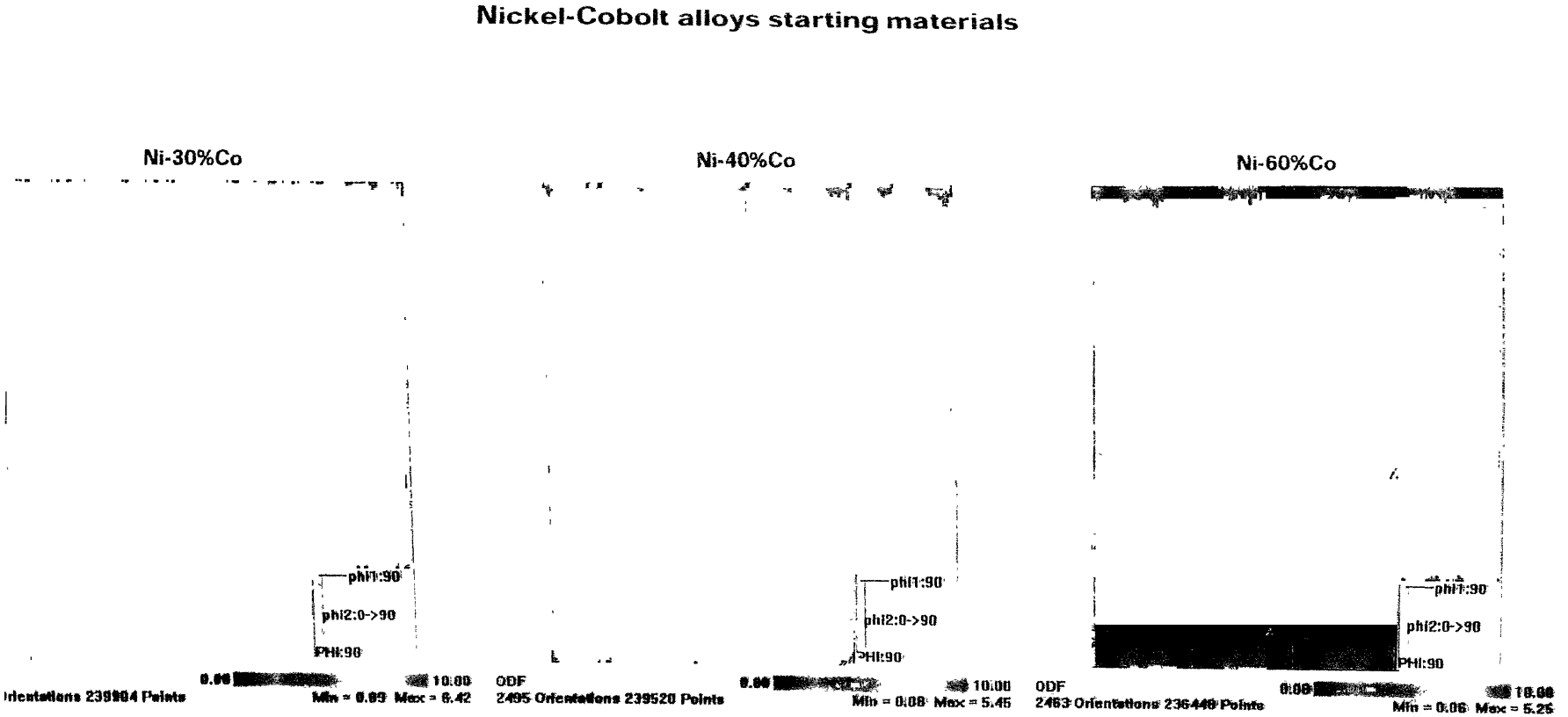

Figure 4.3.1.1 ODF of starting materials of three Ni-Co alloys.

4.3.2 20% Deformed Material

The ODFs of the three 20% deformed alloys are depicted in Figure 4.3.2.1. It is quite clear that in case of the NI-30Co alloy, even after this low deformation, some preferred orientation of the grain has occurred. In fact, the pole densities at the Cu locations (□) have intensified perceptibly, while hardly any change has occurred in the exact B_s location. At best some marginal increase in the intensity of the locations near the B_s can only be observed.

In contrast to the above, there has been a marked increase in the pole density at the B_s locations in the Ni-60Co alloy (Figure 4.3.2.1) whereas there is no change in the pole density intensities at the Cu locations

The behavior of the Ni-40Co alloy lies in between the above two extremes. The ODF of the Ni-40Co alloy practically does not show any change in features exhibited by the corresponding ODF of the starting material.

4.3.3 35% Deformed Material

The ODF of all the three alloys shows a big change after 35% rolling deformations (Figure 4.3.3.1). The intensities of the pole density at the Cu locations show a marked increase in case of Ni-30Co alloy. In fact, it can be said that the Cu component has developed moderately strong in this alloy after 35% deformation. On the other hand there is only a marginal increase of the pole density at the B_s locations.

In contrast to the behavior of Ni-30Co alloy, the ODF of the Ni-60Co alloy shows a sharp increase in the intensity of the pole density at the B_s locations (Figure 4.3.3.1) whereas the intensity of the pole density at the Cu locations can be said to be only very marginal.

As in the case of the 20% deformed material, after 35% rolling deformation also, the behavior of the Ni-40Co alloy lies in between those of Ni-30Co and Ni-60Co alloy (Figure 4.3.3.1). In this case the intensities of the pole density at both Cu and B_s locations have perceptibly improved. The pole densities at both these locations show higher intensities, as compared to the 20% deformed sample of the same material. However, intensities at neither the Cu nor B_s locations, in the alloy, can match with the higher intensity values obtained in the Cu positions for the Ni-30Co alloy and in the B_s position for the Ni-60Co alloy.

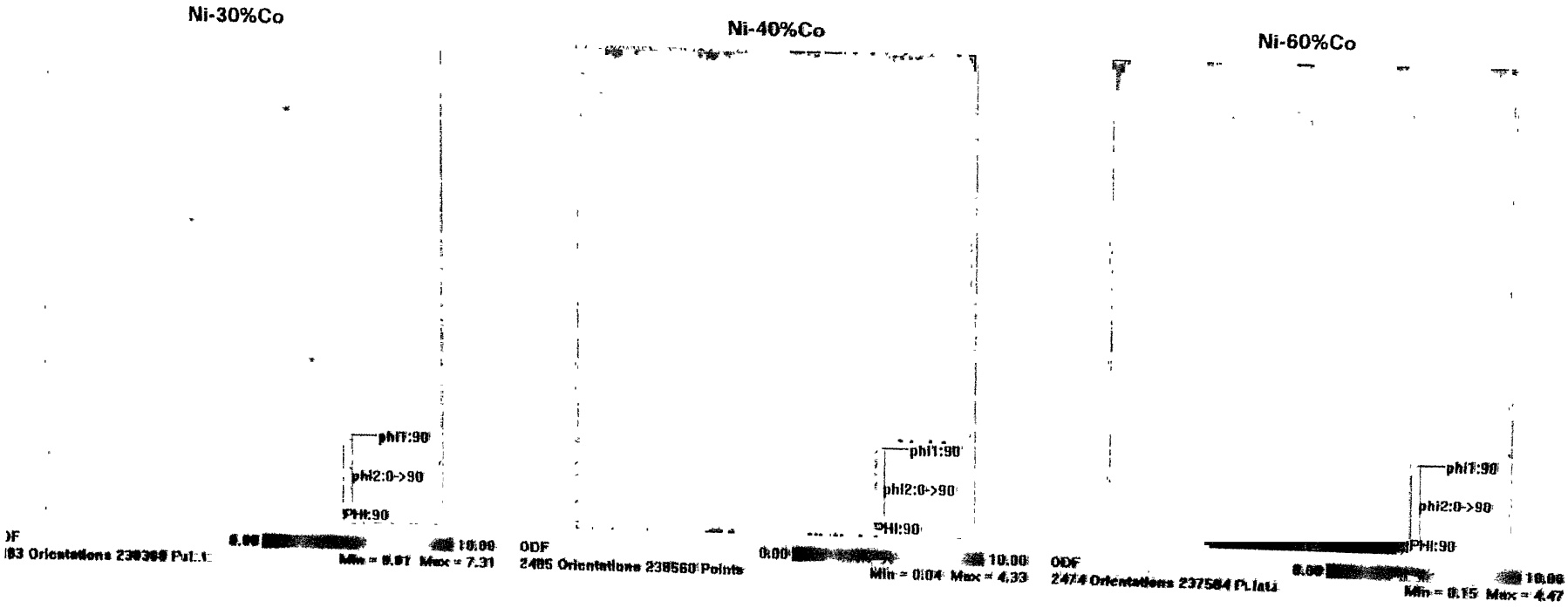

Figure 4.3.2.1 ODF of three Ni-Co alloys at 20% deformation level.

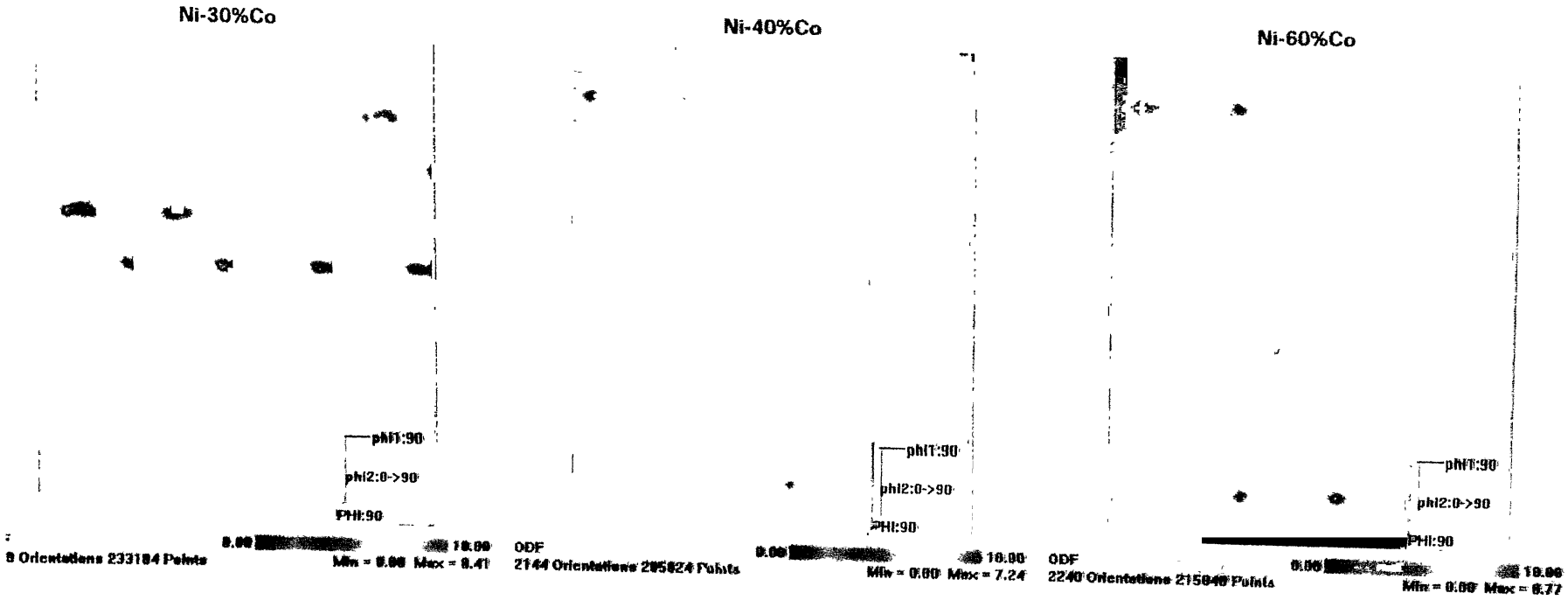

Figure 4.3.3.1 ODF of three Ni-Co alloys at 35% deformation level.

The gradual development of crystallographic textures in the three experimental alloys, as a function of the level of cold deformation, is depicted in Figures 4.3.4.1 to Figure 4.3.4.3. It is quite clear from these diagrams that a pure metal type (or Cu type) deformation texture is produced in the Ni-30Co alloy after a total deformation of 35%, whereas an alloying type (or α brass type) texture is produced in the Ni-60Co alloy. The deformation texture produced in the Ni-40Co alloy is of much lower overall strength and it has characteristic of both pure metal type and alloy type texture.

4.3.5 Microstructure Obtained by Orientation Imaging Mapping (OIM)

A typical microstructure, obtained by the OIM, from the Ni-60Co alloy after 35% cold rolling, is presented in Figure 4.3.5.1. The different color codes used in this micrograph refer to the different crystallographic orientations of the grains. Thus an OIM microstructure incorporates the information regarding the nature of the microstructures as obtained by optical microscopy and, at the same time, gives an idea about the crystallographic orientations of the respective grains. Thus a wealth of information may be obtained from them. The totality of the crystallographic orientation of the grains can be represented in the form of ODFs, which have been shown above.

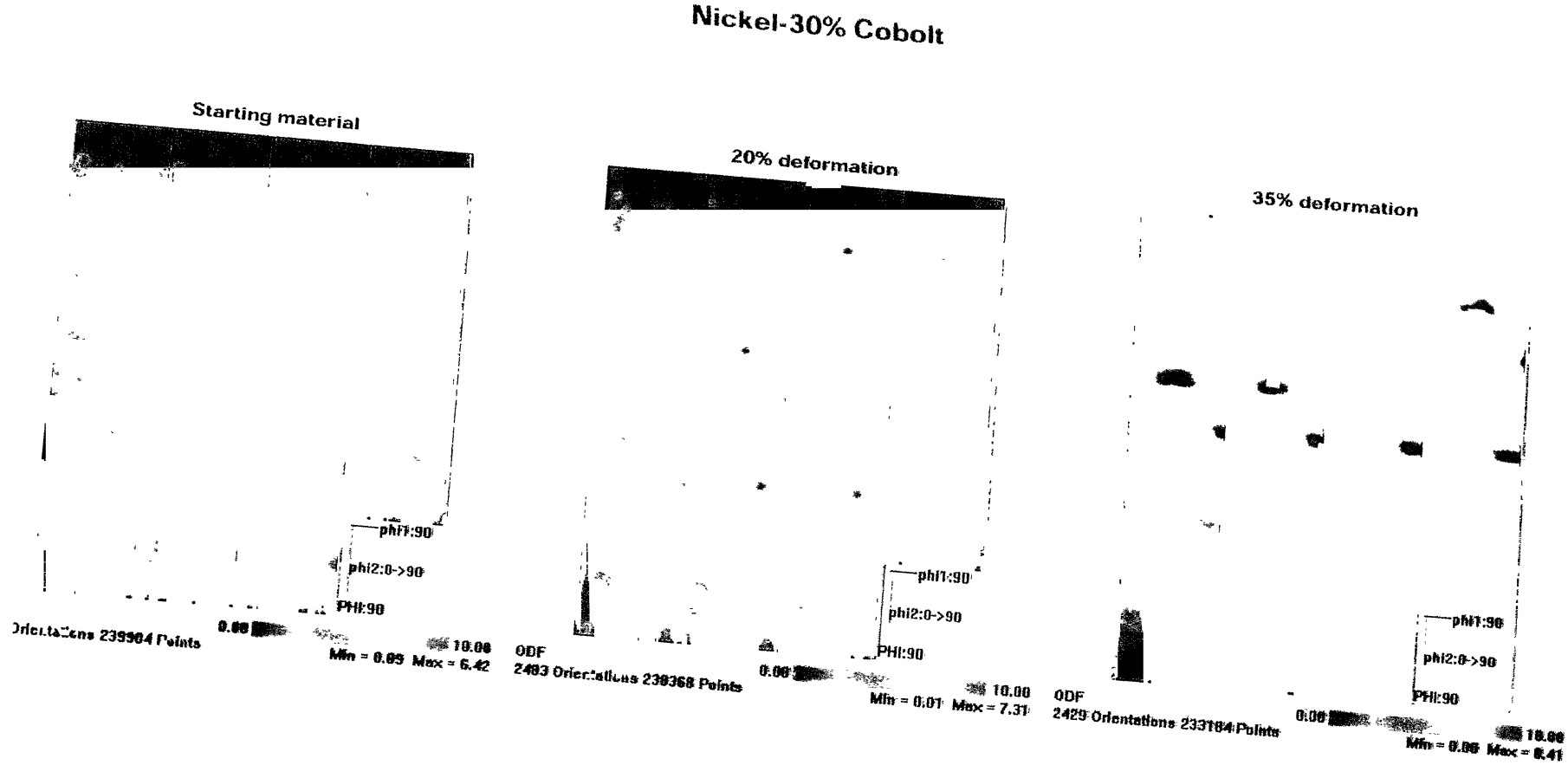

Figure 4.3.4.1 Gradual development of texture in Ni-30Co alloy.

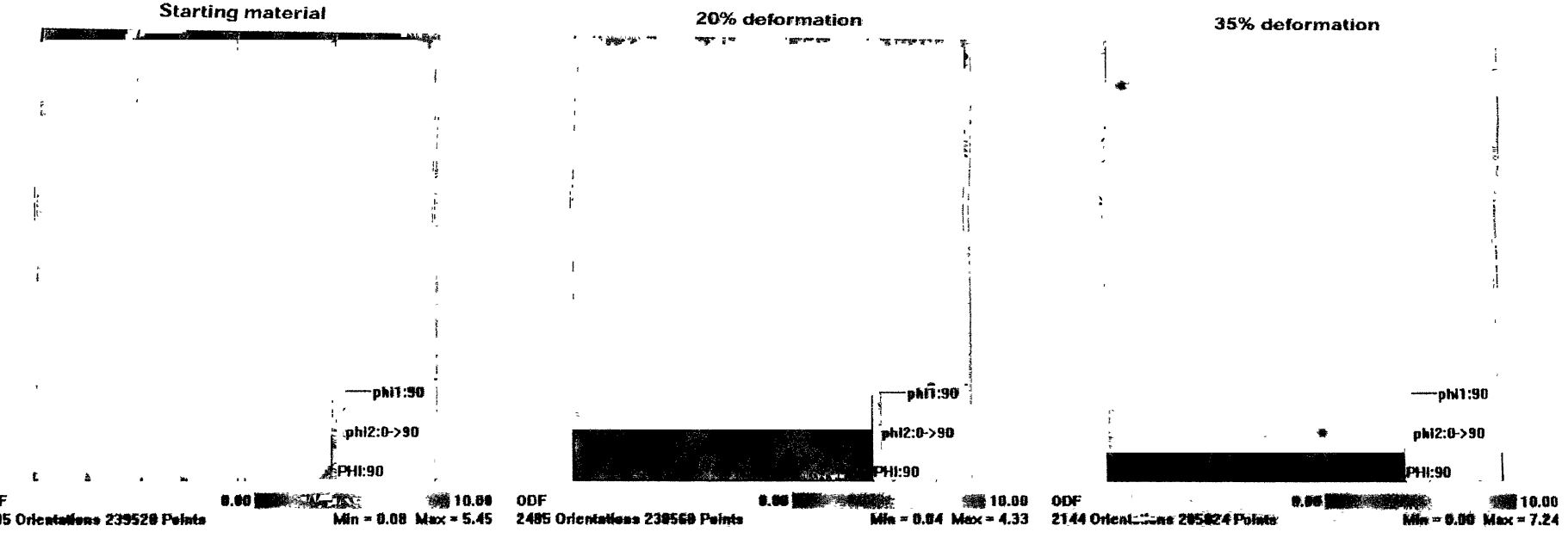

Figure 4.3.4.2 Gradual development of texture in Ni-40Co alloy.

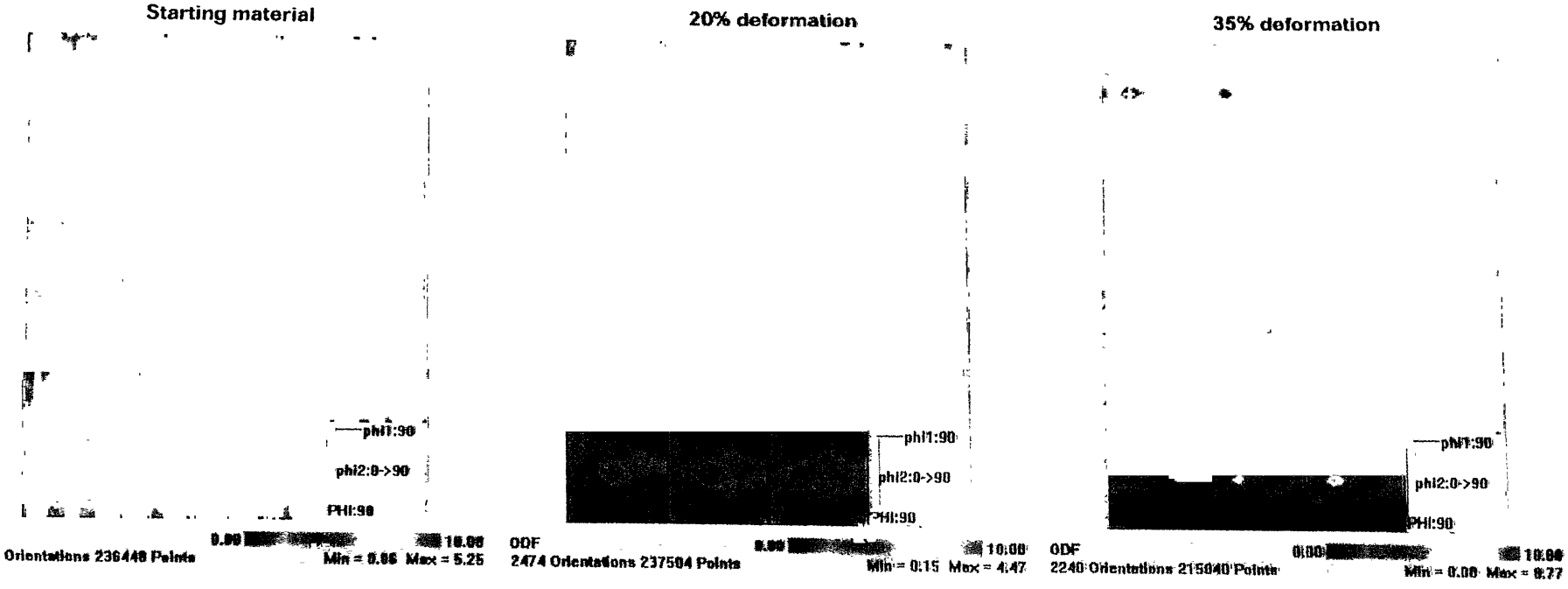

Figure 4.3.4.3 Gradual development of texture in Ni-60Co alloy.

n60c35 1_plot1 (450x483x15b bmp)

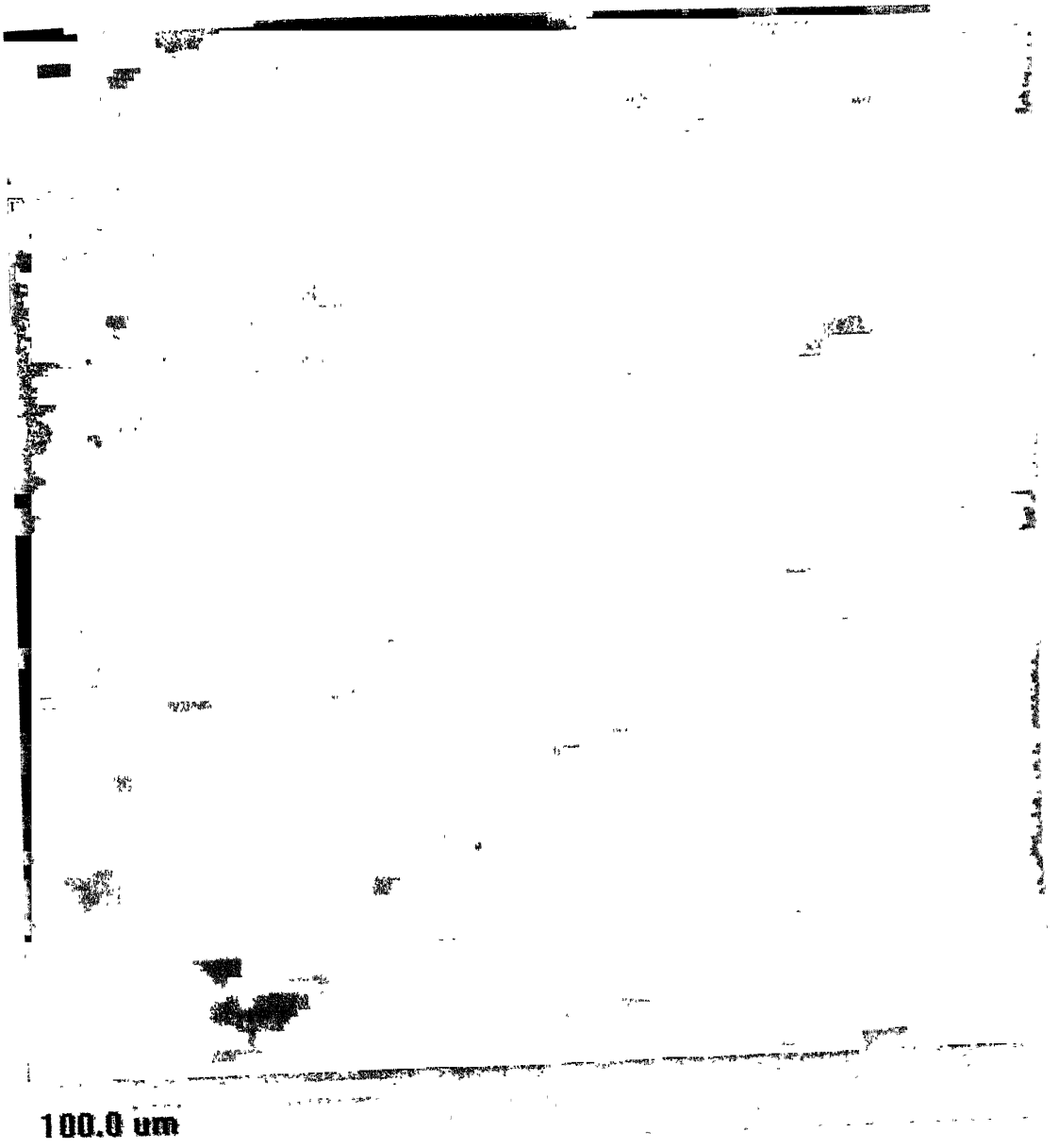

Figure 4.3.5.1 A typical microstructure of 35% deformed Ni-60Co alloy obtained from OIM.

CHAPTER – 5
DISCUSSION

The present work was undertaken to test a commonly accepted theory regarding the deformation texture development in f.c.c. materials of low stacking fault energy, such as α-brass. It is known that high and medium stacking fault energy materials, such as Al and Cu, show a pure metal (or Cu) type deformation texture, characterized by the Cu {112}<111>, B_s {110}<112> and S{123}<634> components. By contrast the low stacking fault energy materials like Cu-30%Zn alloy exhibit an alloy (or α-brass) type deformation texture characterized predominantly by the B_s {110}<112> component. Although a number of theories have been suggested to explain this transition of deformation texture as a function of the SFE of f.c.c. materials, the twinning hypothesis of Wassermann [46] is the most accepted one. According to this hypothesis, all f.c.c. metals and alloys irrespective of their SFEs start developing a pure metal type deformation texture right from the beginning of the deformation process by normal slip on {111} planes. After a particular amount of deformation around 40-50%, twinning becomes an additional mode of deformation, in case of low stacking fault energy f.c.c. materials only. On the other hand, high and medium stacking fault energy materials continue to deform by the slip process as before. On further deformation, as suggested by Wassermann out of three important component of pure metal type texture, the Cu {112}<111> is the one which is most amenable to twinning converts the {112}<111> component to {552}<115> orientation. Further deformation of this twin orientation will then take place on the favorable slip systems, which will rotate the twin orientation into the Goss {110}<112> by further rotation. As a result of this the volume fraction of the B_s component and not much of the Cu {112}<111>, which presumably has been converted into B_s {110}<112> component.

A series of Ni-Co alloys having different values of SFE, from rather high to rather low, were examined by Ray [1] with a view to determine their crystallographic texture after a very heavy amount (95%) of deformation. He observed a pure metal type texture in a Ni-30Co alloy and an alloy type texture in a Ni-60Co alloy while the texture of the Ni-40Co alloy exhibited the characteristic of both the types. The presence of

deformation twins in the TEM micrograph of the heavily deformed Ni-60Co alloy and their absence in the Ni-30Co alloy was considered by him to be the main reason behind the texture transition from alloy with lower Co (30%) to the alloy with high Co (60%) content. This observation coupled with the presence of twinned Cu component {552}<115> in the deformation texture of heavily deformed Ni-60Co alloy, gave credence to the theory proposed by Wassermann to explain texture transition in f.c.c. materials as a function of their SFE.

There have been several objections to Wassermann's hypothesis. In order to convert the entire volume fraction Cu {112}<111> oriented material to B_s {110}<112>, an enormous amount of twinning activity is needed. In fact the volume fraction of the twinned material observed by various workers [51,52] in their TEM studies was never very high. This prompted some criticism of Wassermann's hypothesis. In fact Leffers [52] has suggested for a long time that the differences in deformation texture of high and low stacking fault energy materials could be starting right from the very early stages of deformation process, and not at a latter stage as proposed by Wassermann. Hirsch and Lücke extensively studied the deformation texture development in Cu-Zn alloy, having SFEs varying from 55mJ/m^2 (for pure Cu) to 12mJ/m^2 (for Cu-30%Zn alloy) The SFE of pure Ni is ~130Mj/m^2 and this comes down to ~ 13mJ/m^2 for an alloy of Ni-60Co. Hirsch and Lücke, in their work on Cu-Zn system observed that in the initial stage of cold rolling, upto 40-45% reduction, the texture development is rather similar in pure Cu and Cu-30%Zn alloy. Beyond that deformation level, the texture in the two materials started changing, producing the pure metal type texture in pure Cu and alloy type texture in Cu-30%Zn alloy.

In the present work, deformation texture development in the three Ni-Co alloys, having different SFEs, has been monitored at rather low levels of deformation of 20% and 35%. The idea was to verify Wassermann's hypothesis in the Ni-Co system. Since the NI-60Co has an SFE of ~13mJ/m^2, whereas a Cu-30%Zn alloy, studied by Hirsch and Lücke has an SFE of~12mJ/m^2, it was thought that a good comparison between this two alloys could be made considering the sequence of deformation texture development in them.

The present work has clearly shown that the course of deformation texture development in the Ni-30Co and Ni-60Co alloys are very different from each other. Right

from the early stages of deformation (20% reduction), the pole density shows a perceptible increase at the Cu positions in the Ni-30Co and at the B_s position in the Ni-60Co (Figure 4.3.4.3). Even at this low deformation level no Cu component forms in the Ni-60Co alloy thus ruling out the present the idea that the Cu component forms at the very beginning of deformation in f.c.c. materials of any stacking fault energy. With the increase in the level of deformation (say 35% deformation), the B_s component intensifies in the Ni-60Co alloy. This kind of behavior of the Ni-60Co alloy (SFE of ~13mJ/m^2) is totally different from the Cu-30%Zn alloy (SFE of ~12mJ/m^2) having almost the same SFE. In the latter system substantial amount of Cu component forms at the initial stage of deformation and then it is supposed to go to the B_s position by twinning

Although bundles of deformation twins have been observed in the thin foils of both 20% and 35% deformed Ni-60Co alloy, their total volume fraction does not appear to be very high. Not only that, no Cu twin oriented component could be seen in the ODF of the Ni-60Co alloy at all. Thus, even if Wassermann's hypothesis may hold good for the Ni-30%Zn alloy, the same can't be said to explain the deformation behavior of the Ni-60Co alloy, having similar SFE.

The Ni-30Co alloy, from the very beginning of deformation, shows the development of the Cu component and hardly any B_s. With increasing deformation level the Cu component intensifies substantially. This is similar to behavior of any high or medium SFE f.c.c. material, like Cu or Al etc. Evidently the deformation texture develops in this material by the process of slip only, as no deformation twins could be found in the deformed electron microstructures.

The deformation behavior of the Ni-40Co alloy appears to lie between those of other two alloys, in the sense that both sip and twinning may be responsible for the deformation process. In fact here neither Cu nor B_s component develops to any significant level after low levels of deformation such as 20% and 35%. In that respect Ni-40Co alloy can really be considered as having a transition composition, dividing to distinct regimes of deformation texture development in the Ni-Co alloys.

CHAPTER – 6
CONCLUSIONS

1. Gradual transition of deformation texture from pure metal (Cu type) type to alloy type (α-brass) type occurs in Ni-30Co alloy system depending on the SFE of the alloys.

2. High SFE Ni-30Co develops a Cu component in its deformation texture while low SFE Ni-60Co alloy develops a strong brass component after a rolling reduction of 20%. The intensities of these components in the respective alloys increases after a rolling reduction of 35%. Weak Cu and B_s components develop in the Ni-40Co alloy after 20% and 35% deformation.

3. No distinct Cu component forms in the Ni-60Co alloy at all after 20% and 35% rolling reduction

4. Absence of the Cu type orientation in the Ni-60Co alloy at early stages of deformation suggests that the 'twin hypothesis' of Wasserman may not be true in all the cases.

REFERENCES

1. R.K. Ray, *Acta Metall. Mater.*, v. 43, n. 10., 3861, (1995).
2. J. G. Byrne, 'Recovery, Recrystallization and Grain Growth', p.1, (1965), The Macmillan Co., New York.
3. J. E. Bailey and P.B. Hirsch, *Proc. Roy. Soc.*, v. A267, 11, (1962).
4. W. Bollman, *J. Inst. Met.*, v. 87, 439, (1959).
5. S. Weissmann, T. Imura and N. Hosokawa, Recovery and Recrystallization of Metals, p.241, (1963), Ed. L. Himmel , Interscience Publishers, New York.
6. P.B. Hirsch, 'Physics of Metals', (1975), Cambridge University Presss, Cambridge, UK.
7. B.L. Averbach, M.B. Bever, M.F. Comerford and J.L. Leach, *Acta Met.*, v. 4, 477, (1956).
8. D. Michell, *Phil. Mag.*, v. 1, 584, (1956).
9. D. Michell and F.D. Haig, *Phil Mag.*, v. 2, 15. (1957).
10. R.J. Roe, *J. Appl. Phys.*, v. 36, 2024, (1965).
11. R. O. Williams, *Trans. A.I.M.E.*, v. 242, 105, (1968).
12. L.G. Schulz, *J. Appl. Phys.*, v. 20, 1030, (1949).
13. B.F. Decker, E.T. Asp and D. Harker, *J. Appl. Phys.*, v. 19, 388, (1948).
14. S.L. Lopata and E.B. Kula, *Trans. A.I.M.E.*, v. 224, 865, (1965).
15. L. K. Jetter and B.S. Borrie, *J. Appl. Phys.*, v. 24, 532, (1953).
16. G.B. Harris, *Phil. Mag.*, v. 113, (1952), 113.
17. R.E. Smallman, *J. Inst. Met.*, v. 84, 10, (1955-56).
18. R.H. Richman and Y.C. Liu, *Trans A.I.M.E.*, v. 221, 720, (1961).
19. M. Hatherly, *J. Austr. Inst. Met.*, v. 8, 140, (1963).
20. C.A. Clark and P.B. Mee, *Z. Metallkunde*, v. 53, 756, (1962).
21. F. Haessner, *Z. Metallkunde*, v. 54, 79, (1963).
22. Y.C. Liu and R.H. Lichman, *Trans A.I.M.E.*, v. 218, 688, (1960).
23. I.L. Dillamore, R.E. Smallman and W.T. Roberts, *Phil. Mag.*, v. 9, 517, (1964).
24. H. Hu and R.S. Cline, *J. Appl. Phys.*, v. 32, 760, (1961).
25. H. Hu, R.S. Cline and S.R. Goodman, *J. Appl. Phys.*, v. 32, 1392, (1961).
26. H. Hu and S.R. Goodman, *Trans A.I.M.E.*, v. 227, 627, (1963).

27. S.R. Goodman and H. Hu, *Trans A.I.M.E.*, v. 230, 1413, (1964).
28. R.E. Smallman and D. Green, *Acta Met.*, v. 12, 145, (1964).
29. F. Haessner, *Z. Metallkunde*, v. 53, 403, (1962).
30. R.K.Ray, Ph.D. Thesis, p. 51, (1973), University of Birmingham, UK.
31. M. Müller, Österr Akad Wiss Math-naturw, KI sitz ber, v. 7, 117, (1958).
32. K. Lücke, 7 th Colloque de Metallurgie, Ecrouissage, Restauration, Recristallisation, Paris p. 1-16, (1963).
33. C.S. Barett, 'The structure of metals', 2nd edn., (1952), McGraw Hill., New York,
34. F.A. Underwood, 'Texture in Metal Sheets', (1961), Macdonald Co., London.
35. I.L. Dillamore and W.T. Roberts, Met. Rev., v. 10, 271, (1965).
36. H. Hu, R.S. Cline and S.R. Goodman, 'Recrystallization, Grain Growth and Textures', p.295, (1966). A.S.M., Metals Park, Ohio.
37. F. Haessner, 'Recrystallization, Grain Growth and Texture', p.386. (1966), A.S.M., Metals Park, Ohio.
38. E.A. Calman, *Acta Met.*, v. 2, 865, (1954).
39. J.F.W. Bishop, *J. Mech. Phys. Solids.*, v. 3, 130, (1954).
40. R.F. Braybrook and E.A. Calman, *J. Inst. Met.*, v. 85, 11, (1956-57).
41. F. Haessner, *Z. Metallkunde.*, v. 54, 98, (1963).
42. T. L. Richards and S.F. Pugh, *J. Inst. Met.*, v. 88, 399, (1959-60).
43. Y.C. Liu, *Trans A.I.M.E.*, v. 230, 656, (1964).
44. I.L. Dillamore and W.T. Roberts, *Acta Met.*, v. 12, 281, (1964).
45. G.E.G. Tucker, *J. Inst. Met.*, v. 82, 654, (1953-54).
46. G. Wasserman, *Z. Metallk.*, v. 54, 61, (1963).
47. P.R. Thorton and T.E. Mitchell, *Phil. Mag.*, v. 7, 371, (1962).
48. J.S. Kallend and and G.J. Davies, *Phil. Mag.*, v. 25, 471, (1972).
49. H.J. Bunge, Mathematische Methoden der Texture Analyse, (1969), Academy Press, Berlin.
50. J. Jura and J. Pospiech, *Textures*, v. 3, 1, (1978).
51. T. Leffers and J.B. Blinde-S□rensen, *Acta Metall. Mater*, v. 38, 1917, (1990).
52. T. Leffers, 'Textures of Materials', v. 1, (1996). (Ed.) Z. Liang, L. Zuo and Y. Chu, Proceedings of the Eleventh International Conference on Textures of Materials (ICOTOM – 11), Xi'an, China.

APPENDIX

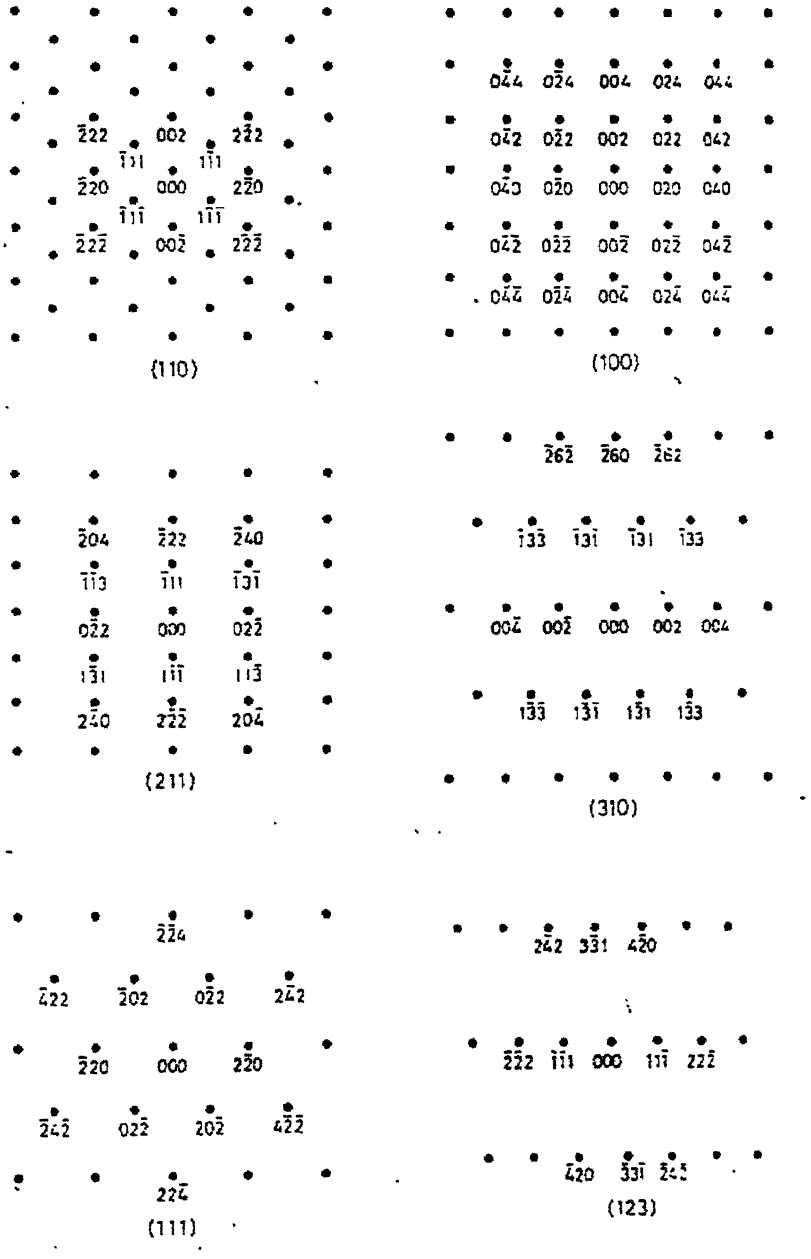

Figure A1 The six most densely populated reciprocal lattice planes for the f.c.c. crystals

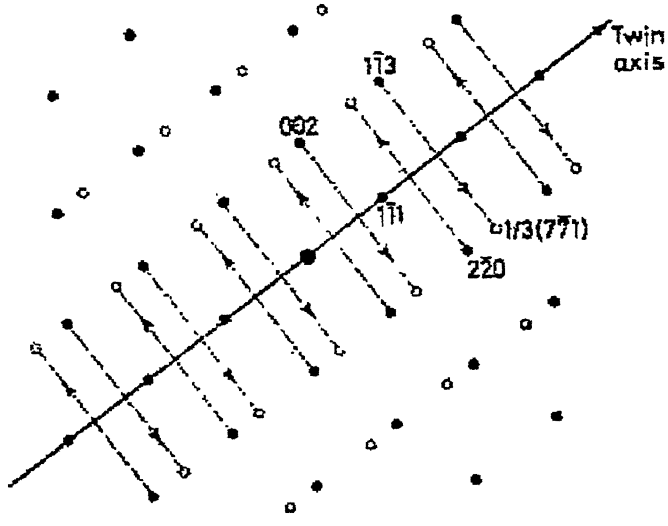

Figure A2 Plotting the twin spots (open circles) due to twinning about an axis lying in the plane of the diffraction pattern. Example shows a f.c.c. (110) pattern with $[1\bar{1}1]$ twin axis.